FIBER OPTIC COUPLERS

G. L. Tangonan

Hughes Research Laboratory
Malibu, CA

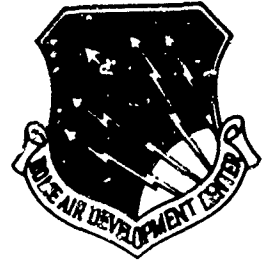Jan 81

RADC-TR-80-358
Final Technical Report
January 1981

FIBER OPTIC COUPLERS

Hughes Research Laboratory

Gregory L. Tangonan

ROME AIR DEVELOPMENT CENTER
Air Force Systems Command
Griffiss Air Force Base, New York 13441

This report has been reviewed by the RADC Public Affairs Office (PA) and is releasable to the National Technical Information Service (NTIS). At NTIS it will be releasable to the general public, including foreign nations.
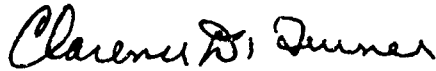
RADC-TR-80-358 has been reviewed and is approved for publication.

APPROVED:

RICHARD PAYNE
Project Engineer

APPROVED:

CLARENCE D. TURNER
Acting Director, Solid State Sciences Division

FOR THE COMMANDER:

JOHN P. HUSS
Acting Chief, Plans Office

If your address has changed or if you wish to be removed from the RADC mailing list, or if the addressee is no longer employed by your organization, please notify RADC (ESO) Hanscom AFB MA 01731. This will assist us in maintaining a current mailing list.

Do not return this copy. Retain or destroy.
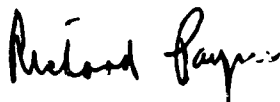
REPORT DOCUMENTATION PAGE		READ INSTRUCTIONS BEFORE COMPLETING FORM
1. REPORT NUMBER RADC-TR-80-358	2. GOVT ACCESSION NO. AD-A097763	3. RECIPIENT'S CATALOG NUMBER
4. TITLE (and Subtitle) FIBER OPTIC COUPLERS		5. TYPE OF REPORT & PERIOD COVERED Final Technical Report 1 Aug 78 – 31 Aug 80
		6. PERFORMING ORG. REPORT NUMBER N/A
7. AUTHOR(s) Gregory L. Tangonan		8. CONTRACT OR GRANT NUMBER(s) F19628-78-C-0201
9. PERFORMING ORGANIZATION NAME AND ADDRESS Hughes Research Laboratory 3011 Malibu Canyon Road Malibu CA 90265		10. PROGRAM ELEMENT, PROJECT, TASK AREA & WORK UNIT NUMBERS 62702F 46001925
11. CONTROLLING OFFICE NAME AND ADDRESS Deputy for Electronic Technology (RADC/ESO) Hanscom AFB MA 01731		12. REPORT DATE January 1981
		13. NUMBER OF PAGES 70
14. MONITORING AGENCY NAME & ADDRESS(if different from Controlling Office) Same		15. SECURITY CLASS. (of this report) UNCLASSIFIED
		15a. DECLASSIFICATION/DOWNGRADING SCHEDULE N/A

16. DISTRIBUTION STATEMENT (of this Report)

Approved for public release; distribution unlimited.

17. DISTRIBUTION STATEMENT (of the abstract entered in Block 20, if different from Report)

Same

18. SUPPLEMENTARY NOTES

19. KEY WORDS (Continue on reverse side if necessary and identify by block number)

Multimode Fiber Optics
Planar couplers
Ion-exchanged waveguides

20. ABSTRACT (Continue on reverse side if necessary and identify by block number)

A planar technology has been developed for fabrication of passive couplers for use in multimode fiber optics. Ion exchange from fused electrolytes has been used for waveguide fabrication using photolithography for pattern definition. Techniques are described for optimizing the throughput of the coupling device when terminated with commercial multimode optical fibers. Couplers have been fabricated in "T", "Y" and star configurations.

DD FORM 1473 EDITION OF 1 NOV 65 IS OBSOLETE
1 JAN 73

EVALUATION

This work is in the forefront of new technology for development of multimode fiber optic couplers. It will have an important impact on fiber communications both within the Air Force and elsewhere. The work is being extended in order to optimize optical throughput and establish the effects of fiber index profile. A successful outcome will allow cheap manufacture of passive couplers which are currently hand-made and expensive.

RICHARD PAYNE
Project Engineer

TABLE OF CONTENTS

LIST OF ILLUSTRATIONS

7

SECTION 1

INTRODUCTION

A.   CURRENT APPROACH TO COUPLER FABRICATION

Multimode fiber-optic systems currently use couplers for data
distribution to several user terminals. Couplers are made by modifying
the optical fibers (fusing, tapering, lapping, and gluing) or with micro-
optic components (such as microlenses and beam splitters). These two
approaches and the planar approach, which was the subject of this pro-
gram, are shown in Figure 1. Good couplers have been demonstrated using
microoptic methods, although several key questions have been encountered
when attempting to transfer the technology to a manufacturing process.

The cost of mass produced couplers is greatly affected by the
reproducibility of the fabrication technique. In the fused fiber
approach, the problem of reproducibility is most severe. Controlling the
electric discharge (or flame torch) conditions and the mechanical devices
for tapering the fused region of the fibers continues to require consid-
erable development. Hughes is actively pursuing techniques to solve
these problems to enable us to manufacture the fused coupler. This work
is pursued by the Hughes Connecting Devices Division at Irvine,
California.

Component placement and packaging in current microoptic devices
requires considerable attention during coupler assembly. Each element
must be antireflection (AR) coated to minimize reflection losses and
maintain high isolation. The cost of the individual components — SELFOC
lenses, beam splitters, and precision machined placement devices — may
prove to be quite prohibitive.

The planar fabrication approach (shown in Figure 1) attacks directly
the problems of reproducibility, one-by-one fabrication, and precise
placement of components which are encountered in the two conventional
approaches by emphasizing the photolithographic control of the coupling
structure and the batch processing capabilities inherent in planar

9

● FUSED COUPLERS

8399-2
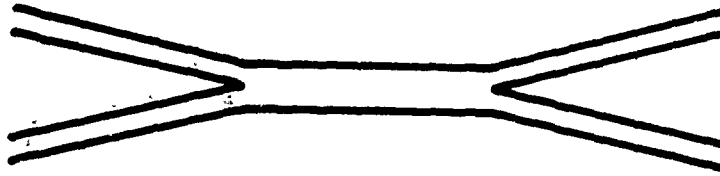
● MICRO OPTIC COUPLERS
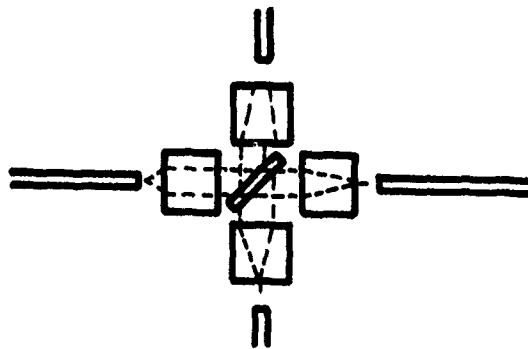
● PLANAR COUPLERS
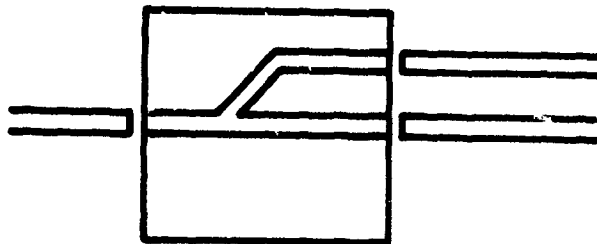
Figure 1.   Schematic of the three approaches to
            coupler fabrication.

10

processing. A schematic of the fabrication process is shown in Figure 2. The basic processing steps illustrated are mask deposition, photoetching for pattern definition, and ion exchange processing. These are techniques that are well developed for processing microelectronics, and the benefits of reproducibility, batch processing, and low cost are obvious. In addition, the positioning of components is largely eliminated by the pattern definition and the use of precision V-groove holders for interfacing the fibers.

The work on this contract emphasized the continued development of the following aspects:

- Field-assisted diffusion to provide step index, high-numerical-aperture (NA) profiles

- Exchange processes in glass which yield high-NA guides (such as Ag into glass)

- Buried channel waveguide coupler formation with low-loss guides and efficient coupling

- Utilization of ray tracing analysis developed at HRL for coupler design

- Utilization of fiber holder technology developed at HRL for interfacing fibers and devices (the silicon V-groove approach).

7320 5

AI MASK DEPOSITION   PHOTOETCHED PATTERN   COMPLETED Y-COUPLER
    (1500 Å)   OF ASYMMETRIC Y-COUPLER   AFTER ION EXCHANGE
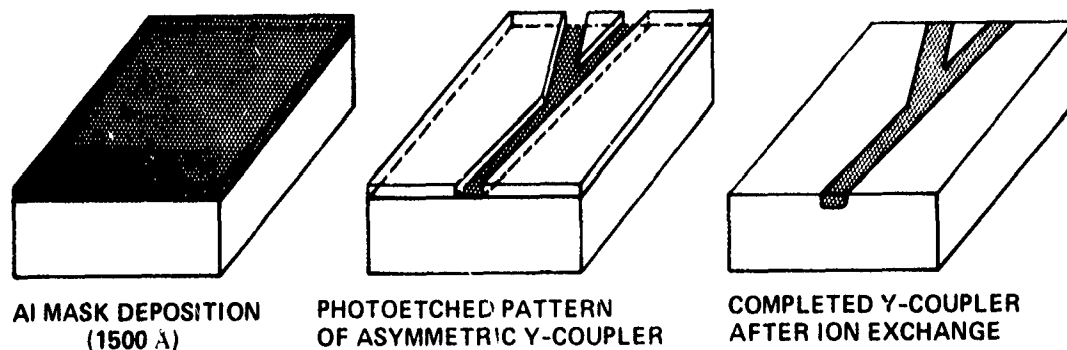
Figure 2.   Masked ion exchange process for coupler
            fabrication.

11

Our approach is based on the recognition of the essential elements required for the optimization of planar couplers. The key elements of our approach are:

- Guide formation process control

- Throughput optimization (fiber to channel to fiber)

- Device design (access couplers, star couplers, splitters)

- Coupler fabrication and fiber interfacing.

Each of these elements has already undergone considerable investigation. The description of the technical approach delineates the areas which were studied and points out where improvements and optimization can be made.

SECTION 2

GUIDE FORMATION PROCESS CONTROL

A. GUIDE FORMATION PROCESSES

Waveguide formation in glass can be accomplished by several techniques, including chemical vapor deposition, ion exchange and diffusion, dip coating, ion implantation, and laser heating. Three years ago, HRL researchers began investigating these various processes for fabricating multimode guides. To date, the preferable approach is clearly ion exchange.

In the past, various ion exchange and diffusion systems have been studied. The approaches we have tried at HRL include:

(1) Li_2SO_2-K_2SO_4 eutectic salt melt/soda lime glass

(2) LiCl-KCl eutectic salt melt/soda lime glass

(3) Ag metal field-assisted diffusion (solid phase)/soda lime glass

(4) $AgNO_3$ melt/soda lime glass (with and without fields)

(5) $AgNO_3$ melt/borosilicate glass (with and without fields)

(6) Double exchange $NaNO_3$ and $AgNO_3$ borosilicate glass.

The most successful ion exchange systems have been (1), (5), and (6). Our description of guide formation gives details of these three processes for the sake of conciseness.

The formation of optical waveguides in planar substrates has been the subject of intensive research in the area of integrated optics. The thrust of these studies has, however, been directed toward single-mode device applications. More recently, multimode fiber optic devices have been made that are quite promising. Auracher et al.[1] reported the first planar branching networks formed in photo-polymer material of 100 µm thickness. Wilson et al.[2] described the use of Ag/Na exchange for coupler formation. More recently, Tangonan et al. of Hughes have described the utilization of ion exchange processes in glass to fabricate couplers,[3] star couplers,[4] and even wavelength demultiplexers.[5]

13

The ion exchange process utilized by the Hughes team in these previous works was that developed by Chartier et al.[6] In this process, a eutectic mixture of Li_2SO_4 and K_2SO_4 is heated under an oxygen atmosphere to $580^\circ C$. A sodium glass slide is suspended over the melt for 30 min. to reach thermal equilibrium with the melt. Next, it is dipped into the melt for 20 min, then is again suspended over the melt for 10 min to avoid any thermal shock. The process is illustrated in Figure 3, along with the phase diagram for Li_2SO_4-K_2SO_4. Planar waveguides, 100 μm deep, are made by this process. The coupler structures are formed by masking with a thick (1 to 2 μm) Al film. The Al mask is subsequently removed by dipping the slide in hot 6 M HCl solution. This process provides an index difference (NA ≈ 0.1) that is too small to cope with larger numerical aperture fibers (NA > 0.2). However, despite this drawback, this process has been quite successful in demonstrating planar processing of coupler devices.

7320 2
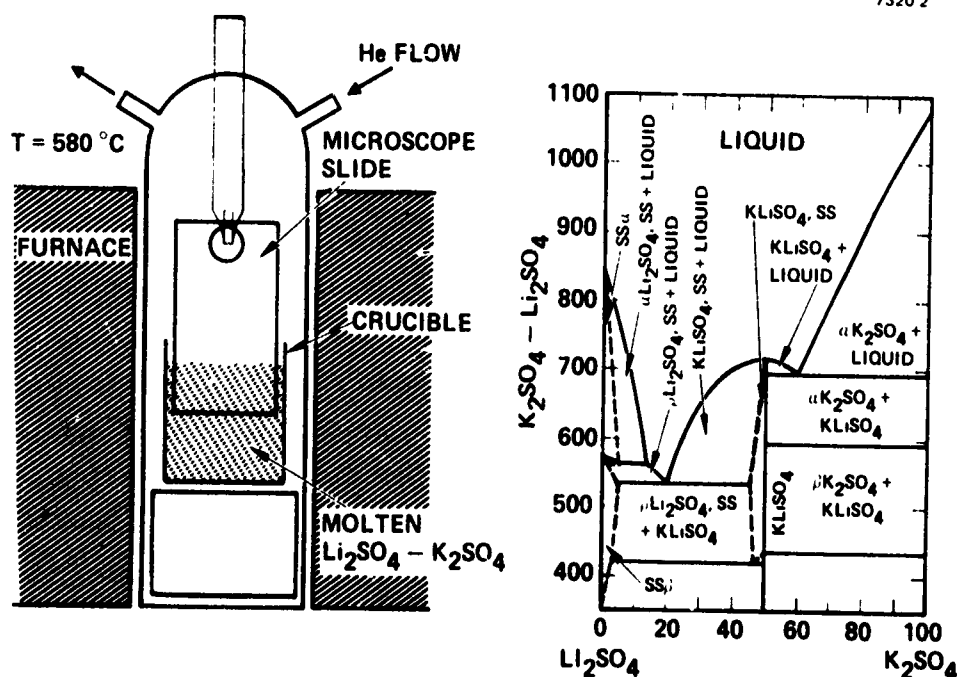
Figure 3. Guide formation processes using Li_2SO_4-K_2SO_4 eutectic melt.

B. FABRICATION OF WAVEGUIDES BY FIELD-ASSISTED ION EXCHANGE

To circumvent the problem of low index of refraction change, an alternative diffusion process was developed: Ag ion exchange under a field. This process is similar to that described by Chartier et al.[7] and Izawa and NaKagome.[8] When ion exchange is carried out in the presence of an electric field, the concentration profiles (and thereby the index of refraction) are considerably modified. The concentration of the ions during the process is given by:

$$\frac{dC}{dt} = D \frac{d^2C}{dZ^2} - E\mu \frac{dC}{dZ} \quad , \tag{1}$$

where the variables C and t are the concentration and diffusion times, respectively, and the diffusion parameters D, E, and μ are the diffusion constant, applied electric field, and the ion mobility, respectively. When the initial concentration of Ag in the glass is zero and an equilibrium surface concentration of C_0 is attained, the resultant profile is given by

$$C(Z,t) = C_0 \, \text{erfc} \left[(Z-E\mu t) / 2 (Dt) \right]^{1/2} \quad , \tag{2}$$

which, for $E=0$, reduces to the result for normal diffusions without a field.

The schematic in Figure 4 shows the concentration profiles attainable by electric field and normal exchange processes. The implications of the profile differences are:

- The field-assisted profile is predominantly a step index with a graded junction into the substrate.

- The product $E\mu t$ essentially controls the depth of the planar step index guide.

The experimental apparatus used to demonstrate electric-field-assisted diffusion is shown schematically in Figure 5. A double-crucible
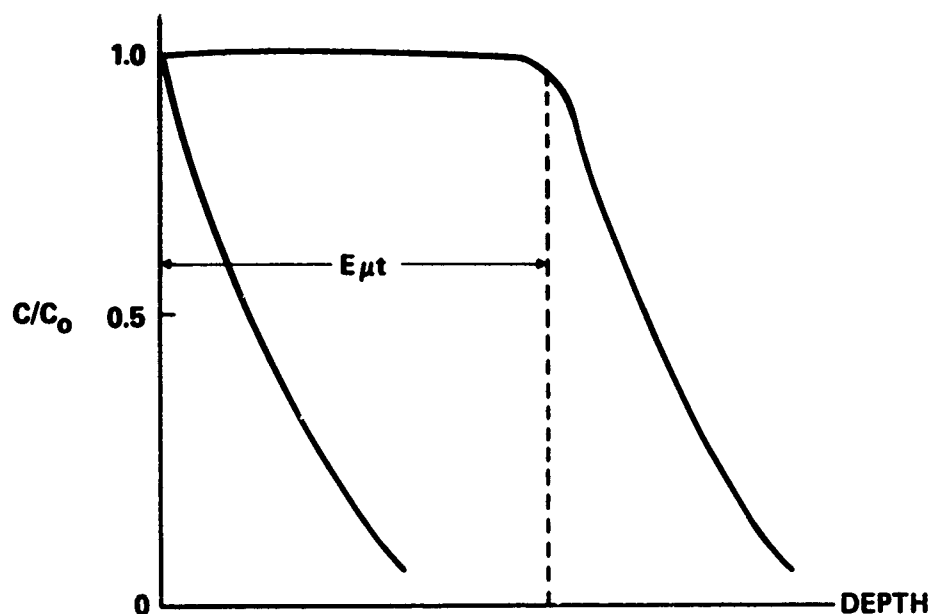
Figure 4. Dif'usion profile obtained with field-assisted diffusion.

arrangement was used to provide a molten salt bath on both sides of the sample. This eliminated Na buildup at the negative electrode side of the substrate. Depending on the polarity of the electrodes, the ion exchange occurs on either side of the sample. Borosilicate glass was used because we found it is readily shaped into the double-crucible configuration, shows little sample warping, and is free from the Ag migration problems observed in soda lime glasses. The parameters used for planar guide formation are given in Figure 6. Deep planar waveguides of low loss are obtained using these parameters. From these results, an approximate measure of the ion mobility of Ag at $370^{\circ}C$ in the glass is given by

$$\mu = 10 \times 10^{-10} \frac{cm^2}{sec \ V} \ .$$ (3)

The index profile obtained for the waveguides was measured using standard interferometric techniques. The result obtained for one of the samples (E) is shown in Figure 7.

16

AgNO₃

RECTANGULAR
BOROSILICATE BOX

a)

Ag⁺

Ag⁺

b)

c)
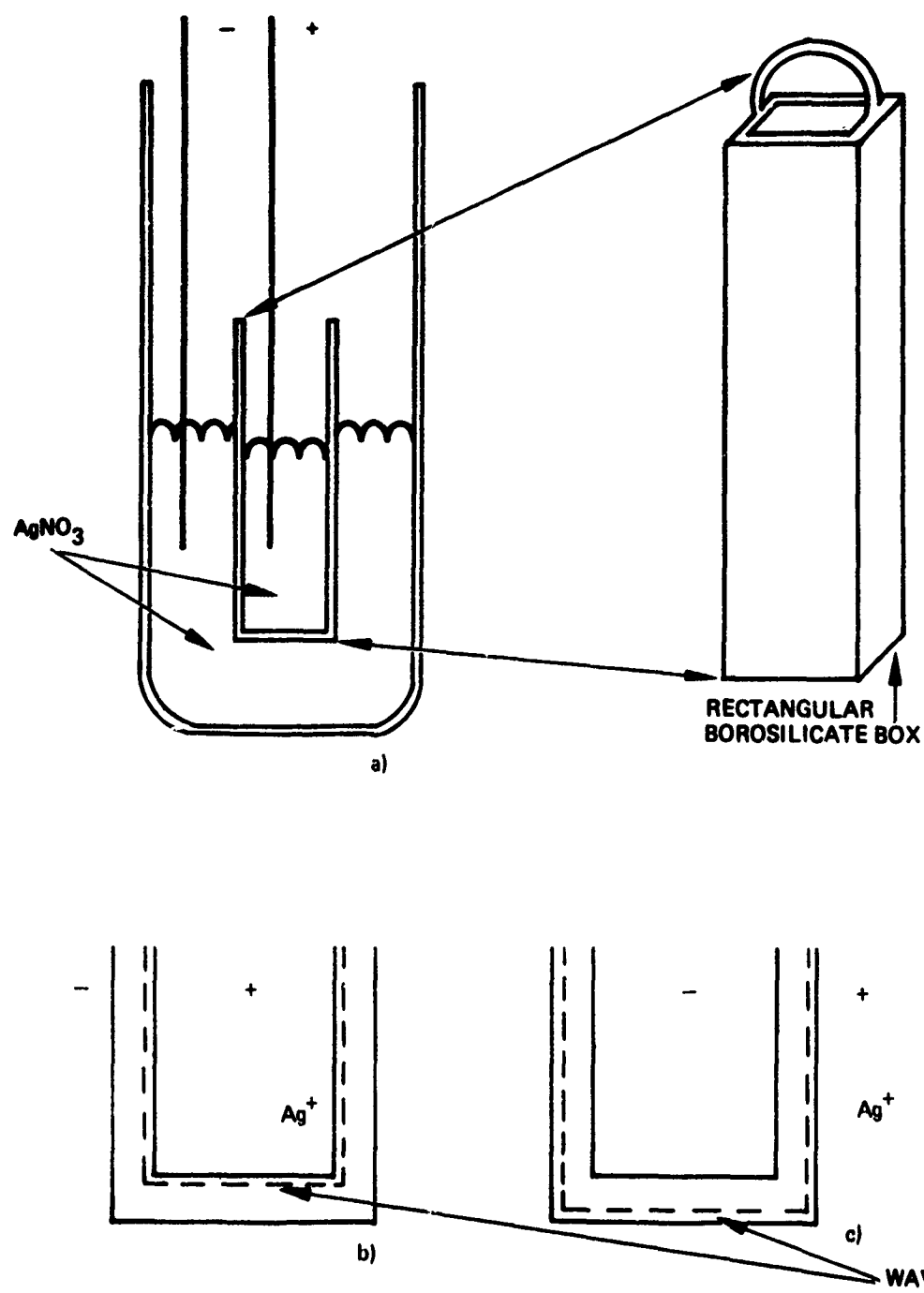
WAVEGUIDE

Figure 5. Double crucible apparatus for guide formation (a);
depending on the polarity of the electrodes, guide
formation occurs on inner (b) or outer (c) surface.

17

SAMPLE	T, °C	t, HR	E, V/MM	I, mA	WAVEGUIDE DEPTH, μm
A	370°C	4.5	33	–	52
B	370°C	1.0	100	–	55
C	370°C	2.5	50 – 230	10	25
D	370°C	3.0	50	–	70
E	300°C	4.2	150	–	35

Figure 6.   Waveguide depth for Ag ion exchange versus
temperature, time, and applied field.
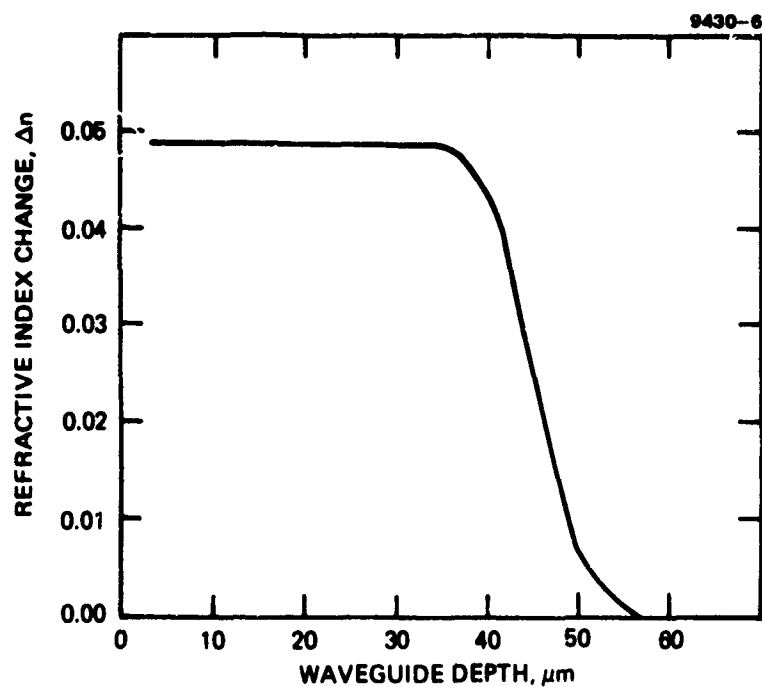
Figure 7.   Index of refraction profile for sample
E.   Note the step-like index profile
measured by interferometric methods.

18

C. BURIED WAVEGUIDE FORMATION

Buried waveguides have been formed by a second field-assisted exchange process using $NaNO_3$. In this process, Na is reintroduced in the surface of the planar guide by the exchange process. A lowering of the index of refraction at the surface is shown in Figure 8. Waveguiding experiments show that the additional confinement layer at the surface shows a dramatic difference in optical waveguide output profile. This output of two guides, with and without burying, is shown in Figure 9.

D. CHANNEL WAVEGUIDE BURYING

Channel waveguides can be formed by using an aluminum mask for blocking the exchange process. Channel waveguides formed in this way can be buried using the same process described above.[9] A comparison of the output profiles for two waveguides formed with and without burying is shown in Figure 10. A clear difference is observed between the two waveguide output profiles. In the laboratory, the buried waveguides show a remarkable uniformity along the length of the guides when excited by light. This is in contrast to the case of the unburied guides, in which surface scattering due to cracks and polishing scratches is seen as bright scattering sites.

E. APPLICATIONS POTENTIAL OF PLANAR COUPLERS

Based on previous results,[3,4] the major problem area in exploiting the planar coupler is to reduce the coupling losses encountered in mating input and output fibers with the coupling structure. In recent experiments on Ag ion exchange samples, major improvements in the throughput from fiber to channel to fiber have been demonstrated. For unburied guides, the throughput loss is as low as 1.1 dB. For buried guides, losses of <1 dB have been measured. This result makes planar coupler structures quite competitive with conventional fusion approaches. That a variety of structures can be made by photolithographic control of the diffusion masks has already been established by our previous results.[3,4]

9430-8

NaNO$_3$
~ 350°C

$\oplus$

A$_8$NO$_3$

$\ominus$
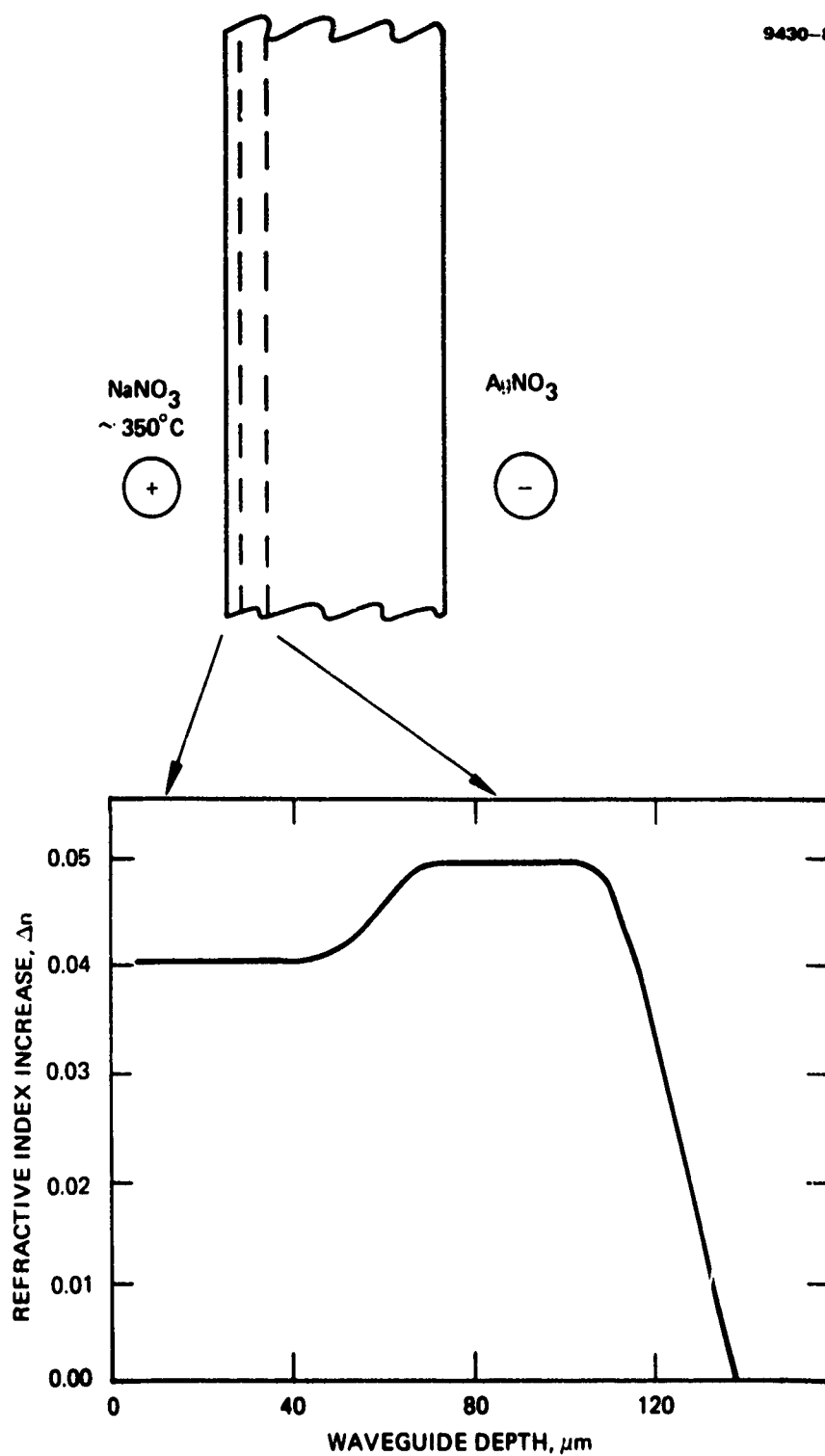
Figure 8.   Double exchange formation of buried waveguides.
The burying is incomplete, although the index
drop of 0.01 is still substantial.

20

9748-2

SURFACE
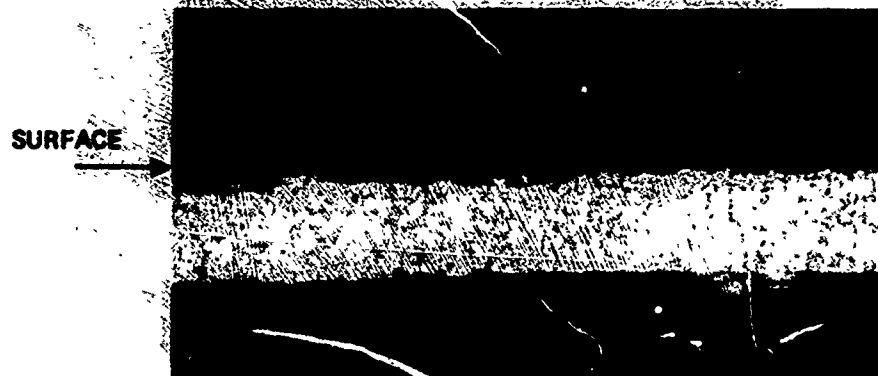
DEPTH = 180 μm
Ag DIFFUSION : 300°C, 4 hr, 30 V/mm

SURFACE

DEPTH = 50 μm
Ag DIFFUSION: 300°C, 1 hr, 30 V/mm
Na BURYING: 400°C, 1 hr, 25 V/mm

Figure 9.   Buried planar waveguides compared to unburied
            guides. Processing: Ag diffusion (300°C, 1 hr,
            30 V/mm) and Na diffusion (400°C, 1 hr, 25 V/mm).

21
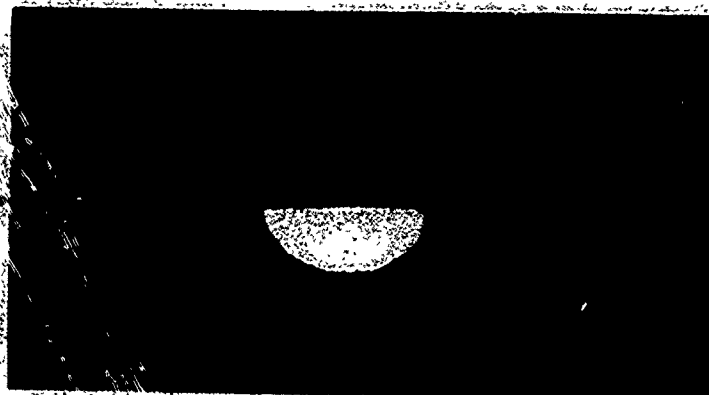
SURFACE

GUIDE – 160 μm x 80 μm
MASK – 27 μm
Ag DIFFUSION – 300°C, 60 min,
150 V/mm

SURFACE

GUIDE – 160 μm x 80 μm
MASK – 25 μm
Ag DIFFUSION – 300°C, 30 min,
150 V/mm
Na BURYING – 400°C, 30 min,
30 V/mm

Figure 10.   Buried channel waveguides (160 μm x 80 μm)
             compared to unburied guides. Processing:
             25 μm mask width, Ag diffusion (300°C, 30 min,
             150 V/mm) and Na burying (400°C, 30 min,
             30 V/mm).

F. PROBLEM AREAS AND OPTIMIZATION

We anticipate several problems in the area of materials processing which should be further studied. The problems which should be investigated are:

- Incomplete burying of the waveguides with current techniques

- Edge effects during masked ion exchange which cause the thickness variations of the waveguides

- Optimization of buried channel guides for high throughput efficiency

- Improvements in temperature and field control throughout the diffusion process.

The first two of these problem areas require elaboration. Incomplete burying of the waveguides can be deleterious if the effective index barrier for the buried interface is too low. Presently, the surface index difference is 0.01. This should be increased to at least 0.015, so that optical fibers with numerical apertures of >0.20 can be accommodated. Our subsequent investigations should concentrate on varying the diffusion conditions to increase the confinement. It is quite possible that melts other than $NaNO_3$ may be useful.

Th second problem area, edge effects caused by diffusion through a mask, is illustrated in Figure 11. For the same diffusion conditions, the effective diffusion depth varies depending on the position relative to the mask. (The results shown are in fact for the same sample.) This effect depends on the mask width also. The planar guides (no mask) are remarkably thinner than are guides formed through a mask. The contrast in results for wide and narrow masks is also quite interesting. For the wide mask (500 µm), the tendency for thinner guide depths is observed at the center of the guide region. Near the mask edges, an enhanced diffusion is observed. For the narrow mask (35 µm), the expected semicircular profile is observed. Chartier et al.[10] recently reported similar observations. Their explanation of the observed shape of the profiles is based on an electrochemical bias between the silver nitrate bath and the
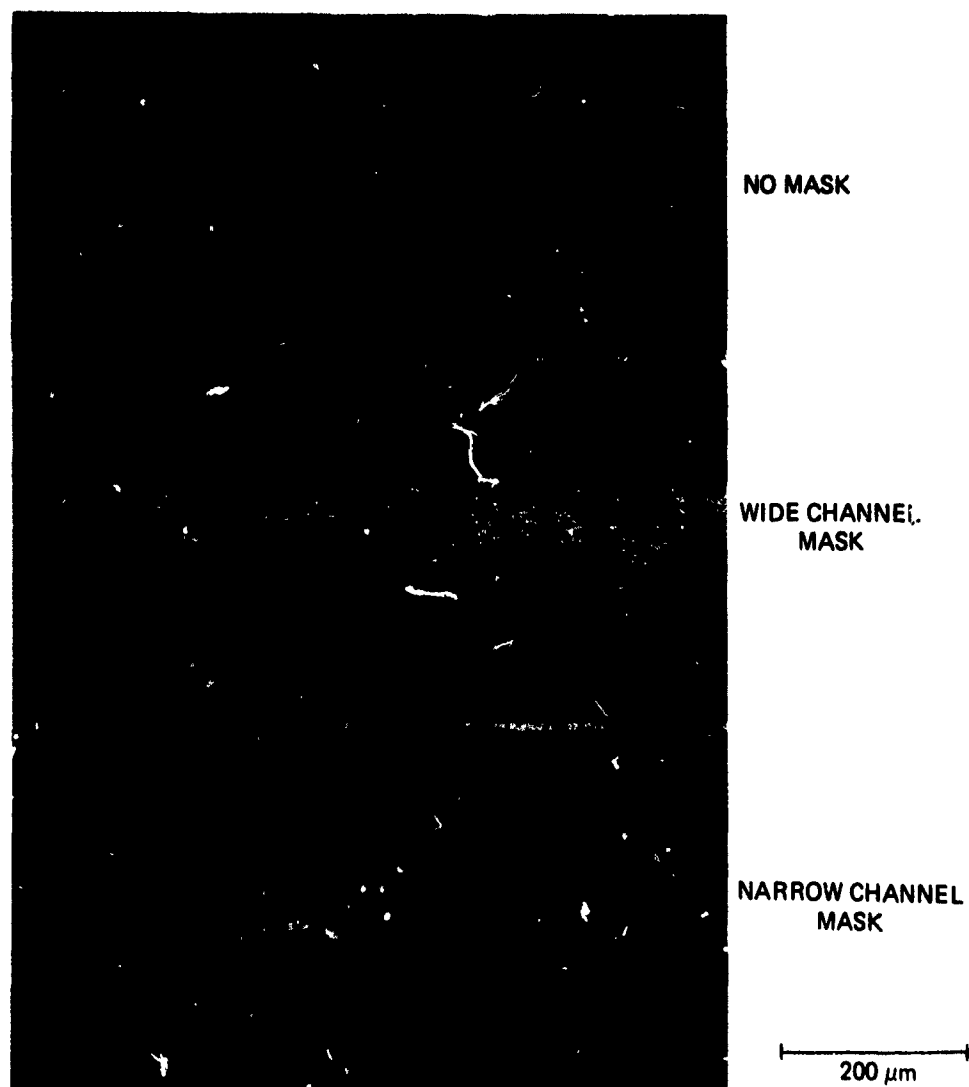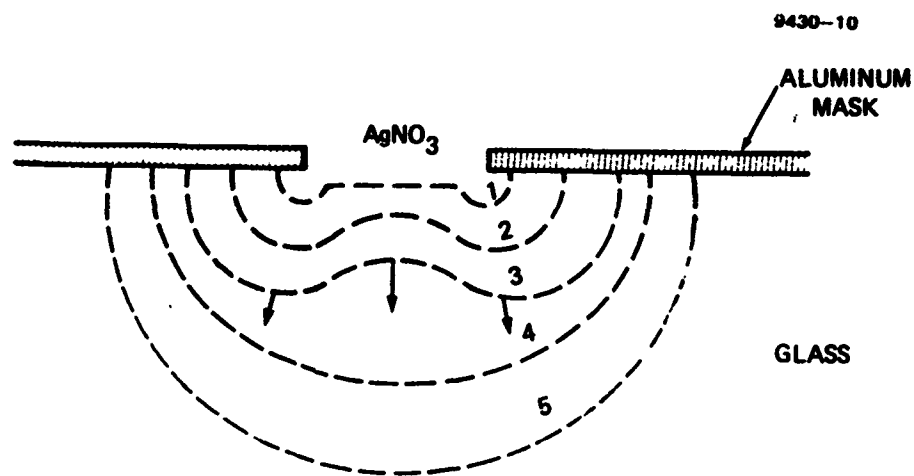
Figure 11. Effects caused by enhanced diffusion at the mask edge (Al).
Note the variation in guide depth with mask width.

metallic mask. An electric field is, in their interpretation, generated by this electrochemical bias.

Current work at HRL differs significantly from Chartier's interpretation. We have replaced the metallic mask (Al) with a nonconducting mask (SiO_2) and studied the edge effects. Almost identical results have been measured However, these results are complicated by the incomplete blocking of the SiO layer. The waveguide profile for the SiO_2 mask is shown in Figure 12. The same diffusion conditions were used to closely compare to the results obtained with the metallic mask. Detailed measurement of the guide shape shows very close similarities. When viewed in the light of the experiments, the interpretation of Chartier et al. may be in error, since the same effects are observed for what should clearly be different electrochemical systems.

9807—3

t = 30 MIN
E = 166 V/M
W = 500 μm
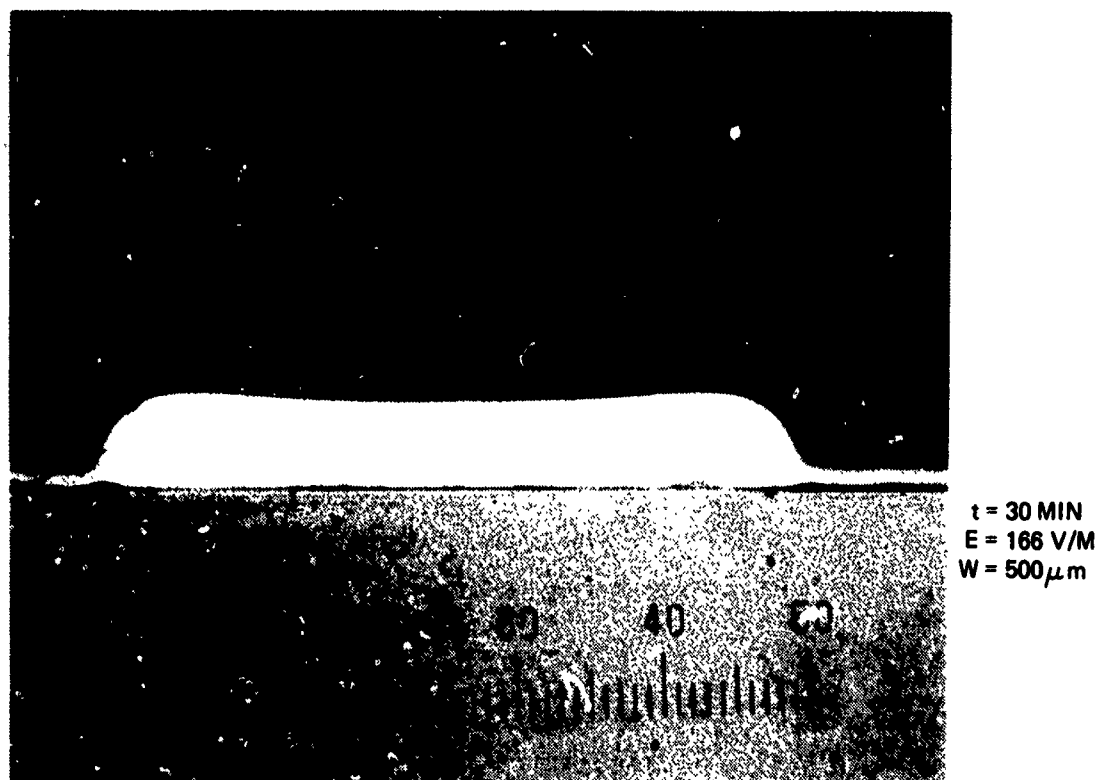
Figure 12. SiO_2 mask results.

Our current interpretation is that the observed results are simply due to current spreading effects at the mask edge. We plan to continue to investigate this effect during the proposed program.

The technical significance of this problem cannot be min.mized. The fabrication of star couplers, which require very wide masks (several mm) to form the mixing region, will be complicated by the guide thinning effects. Fortunately, the high index guides we have used are highly overmoded (very high NA) when compared to the excitation conditions using conventional fibers (NA $\simeq$ 0.2). Guide thinning effects may not severely affect star performance, but a closer examination will be necessary.

SECTION 3

THROUGHPUT OPTIMIZATION

A. THE OPTIMIZATION PROCESS

Clearly the most important parameter for gauging coupler performance is the maximum attainable throughput, or, equivalently, the minimum excess loss. The important technical issues for achieving high-performance couplers are the achievement of high coupling efficiency from fiber to channel to fiber (F/C/F), low waveguide absorption and scattering losses, and low internal losses due to branching. Since these issues are clearly paramount in the minds of the ultimate users of planar couplers, our efforts have emphasized throughput optimization.

Although a theoretical analysis of the coupling efficiency could be attempted, we feel that experimental techniques are a superior approach to optimum coupling. More often than not, the theoretical parameters required by an analyst are not in fact readily accessible. The extent to which diffusion conditions can in practice be varied is quite narrow.

Our results on throughput optimization have been taken with conventional optical fibers. Both step- and graded-index fibers have been studied. Depending on the exchange process used for guide formation, the results can be classified into three groups:

- $Li_2SO_4 - K_2SO_4$ guides

- $AgNO_3$ field-assisted guides

- $AgNO_3/NaNO_3$ field-assisted buried guides.

To optimize throughput, we have used a three-step process:

- Variation of the diffusion temperature, diffusion time, and applied field for a reasonably close first set of parameters (given set of mask openings and fiber diameter)

- Second variation of diffusion time and field for a selected group of mask openings (temperature fixed)

- Variation of the buried guide formation parameters (temperature, time, and field) for improved throughput.

27

Setting the temperature to a definite value after the first trial assists in the handling of the molten salt baths and is an experimental preference. By limiting the mask width experiments to a practical range, we can lessen the number of coupling measurements that are required for the tests of structures after step 2 (nonburied guides) or step 3 (buried guides).

Throughput measurements were made in a straightforward manner using carefully cleaved fibers. Mode strippers were used to ensure that only guided mode coupling was being measured. In the cases of high throughput (field-assisted Ag guides — nonburied and buried), index matching fluid was used. This is a reasonable approach since in practice index-matching epoxy will be used to attach the fibers. The fibers were manipulated on x-y-z stages to obtain maximum throughput. In most cases, 10 or more sample guides were prepared for each mask opening to afford a reasonably large sampling. All the throughput data for the Ag-diffused guides were measured at 0.63 μm, while data on the Li-diffused guides were taken at 0.63 μm and 0.85 μm with nearly identical results.

B. THROUGHPUT RESULTS ON Li_2SO_4-K_2SO_4 GUIDES

Detailed measurements were made of the throughput of guides formed by the ion exchange of soda lime glass in Li_2SO_4-K_2SO_4 eutectic salt baths. The results of the optimization process (involving steps 1 and 2) are summarized in Figures 13 and 14. The total throughput loss for the best case was -4.2 dB (F/C/F). By collecting all the output light of the guide by using a lens, measures of the fiber-to-channel coupling (F/C) and of the channel-to-fiber coupling (C/F) were obtained. Note that the F/C data include the propagation loss over 1 to 2 cm of guide.

The results for the Li_2SO_4-K_2SO_4 guides demonstrate low throughput. The index of refraction profile for these guides is not optimal in two aspects: they exhibit low effective numerical aperture (NA < 0.1) and have a linearly graded index of refraction. This result suggested that a definite advantage would be gained by achieving high-index guides.

F/C

CHANNEL

FIBER   LENS   DETECTOR

P_{IN} P_{OUT}

■ FIBER-CHANNEL (F/C)

$P_{IN} = 185\,\mu W$
FIBER, GRADED
CORE, $63\,\mu m$ DIAM
FIBER, $125\,\mu m$ DIAM

F/C/F

CHANNEL

FIBER   FIBER   DETECTOR

P_{IN} P_{OUT}

● FIBER-CHANNEL-FIBER (F/C/F)

AI MASK

~$100\,\mu m$

GLASS
SUBSTRATE

LIMIT OF ION EXCHANGE

CHANNEL
GEOMETRY $63\,\mu m$
FIBER CORE

P_{OUT}/P_{IN}, POWER RATIO, %

(MASK) CHANNEL WIDTH, $\mu m \rightarrow$
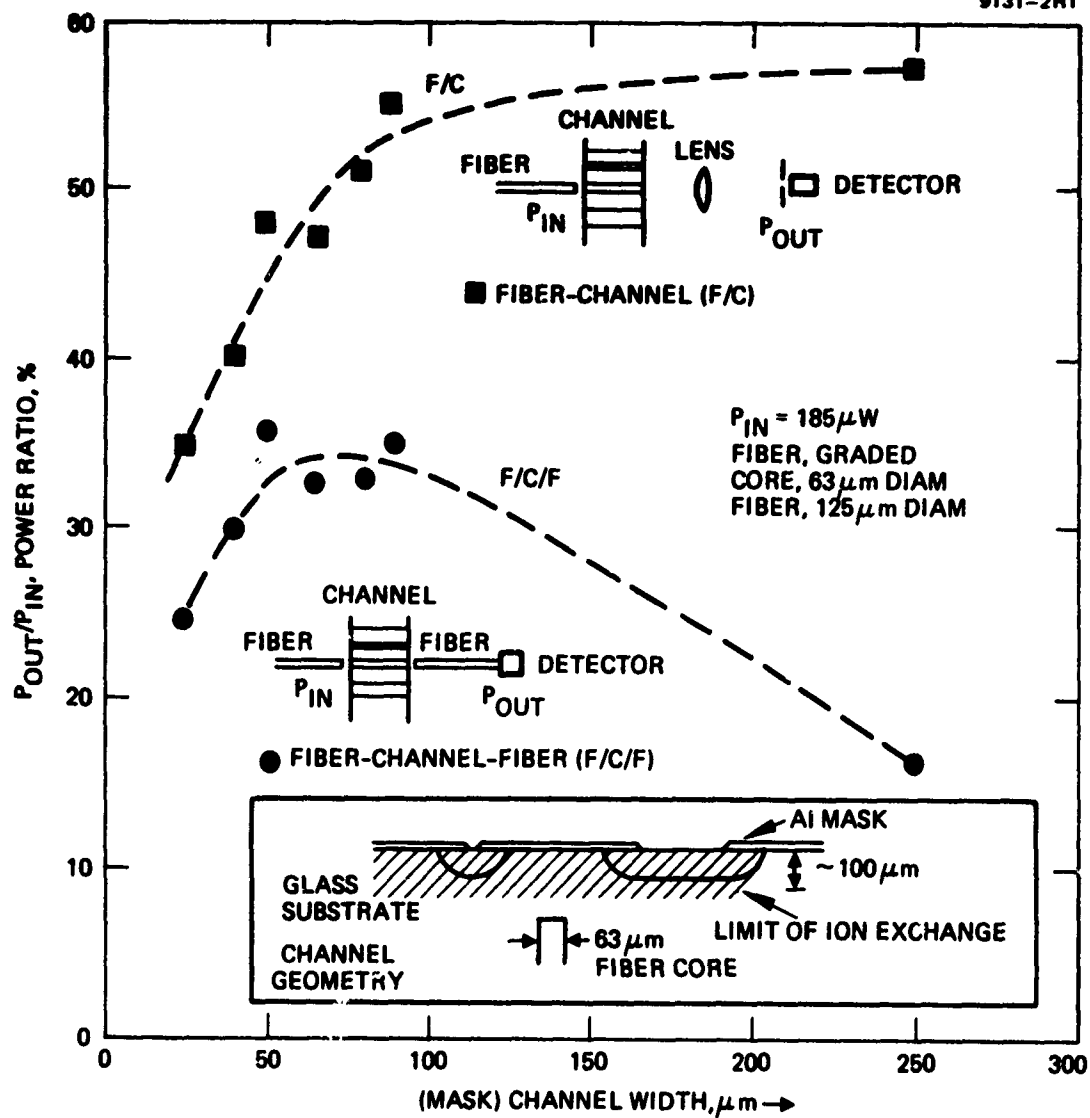
Figure 13. Power transmission ratios of constant
length channels versus channel width.

29
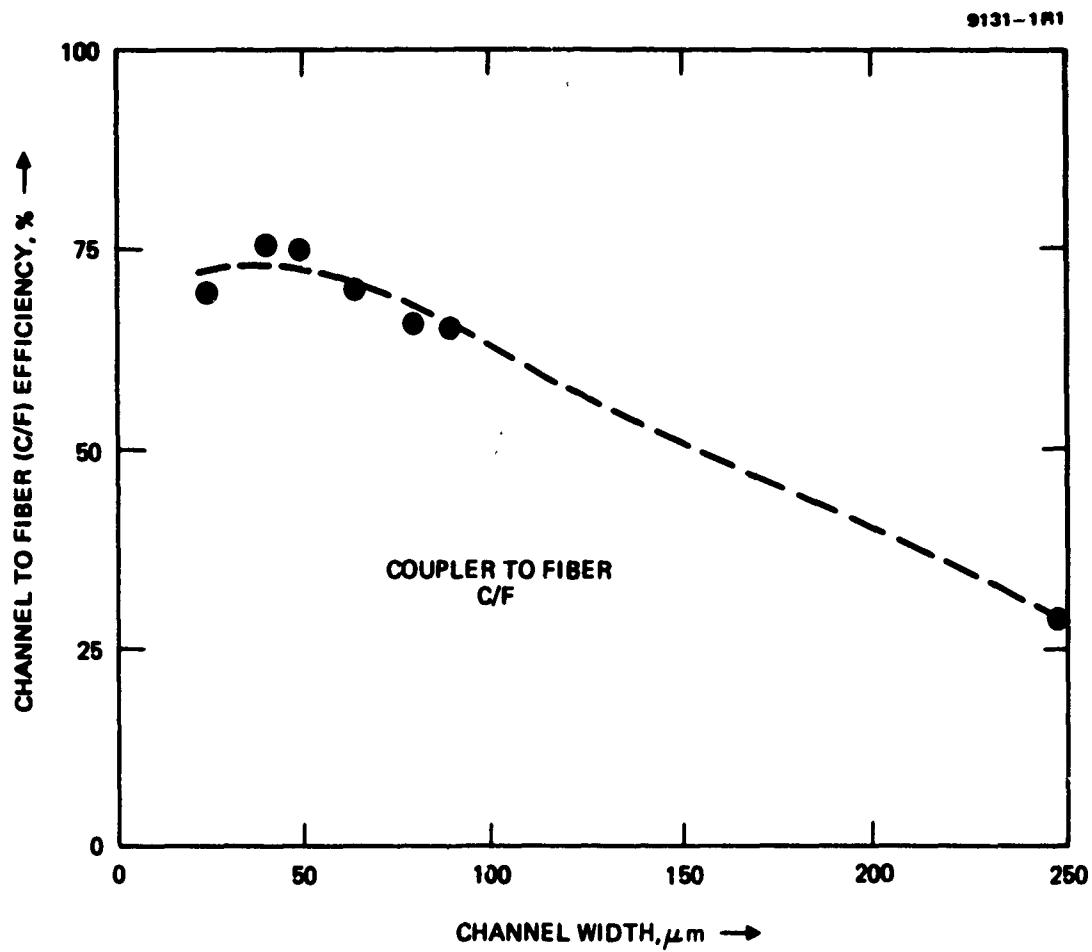
Figure 14.   Channel-to-fiber coupling efficiency versus channel width.

Waveguide losses, while difficult to measure, are felt to be quite low (≈0.1 dB/cm) because of the very high quality of the guides. The degree of variation of the throughput results appears to be caused by surface imperfections (scratches and microcracks). For this reason, buried waveguides were considered a preferable alternative which should be pursued in further work.

C. THROUGHPUT RESULTS FOR FIELD-ASSISTED ION EXCHANGE GUIDES

The results of throughput measurements on channel guides formed by field-assisted Ag exchange are summarized in Figure 15. Considerable improvement over the results for Li exchange was achieved; in fact, these are state-of-the-art results. The data point is the average of measurements on 10 different samples of the same mask width, and the variation signifies the full extent of the process-induced differences as well as fiber placement errors. For some diffusion apertures, the variation is <0.2 dB. The presence of surface defects would account for the spread.

The high throughput for very good samples, in the -1.3 to -1.1 dB range, is most encouraging. These are the best results we have obtained for nonburied guides. The guide length was 1 cm, which is sufficient for planar couplers (access and splitters).

A broad minimum exists for the throughput loss as a function of mask width. This is very important because it signifies that the process control requirements for optimum coupling may not be too strict in the final stage of development. This, of course, must be studied further.

In further work, we will extend these studies to measurements of F/C and C/F coupling and waveguide loss. Losses in the 0.85 to 1.25 μm wavelength range will also be studied. We expect that absorption does add to the waveguide loss in the visible (due to the slight coloration) and that the absorption will be quite low in the IR region. The effects of higher NA (0.25 to 0.30) excitation will be interesting since there is a definite trend toward high NA fibers and LEDs for short links.

31
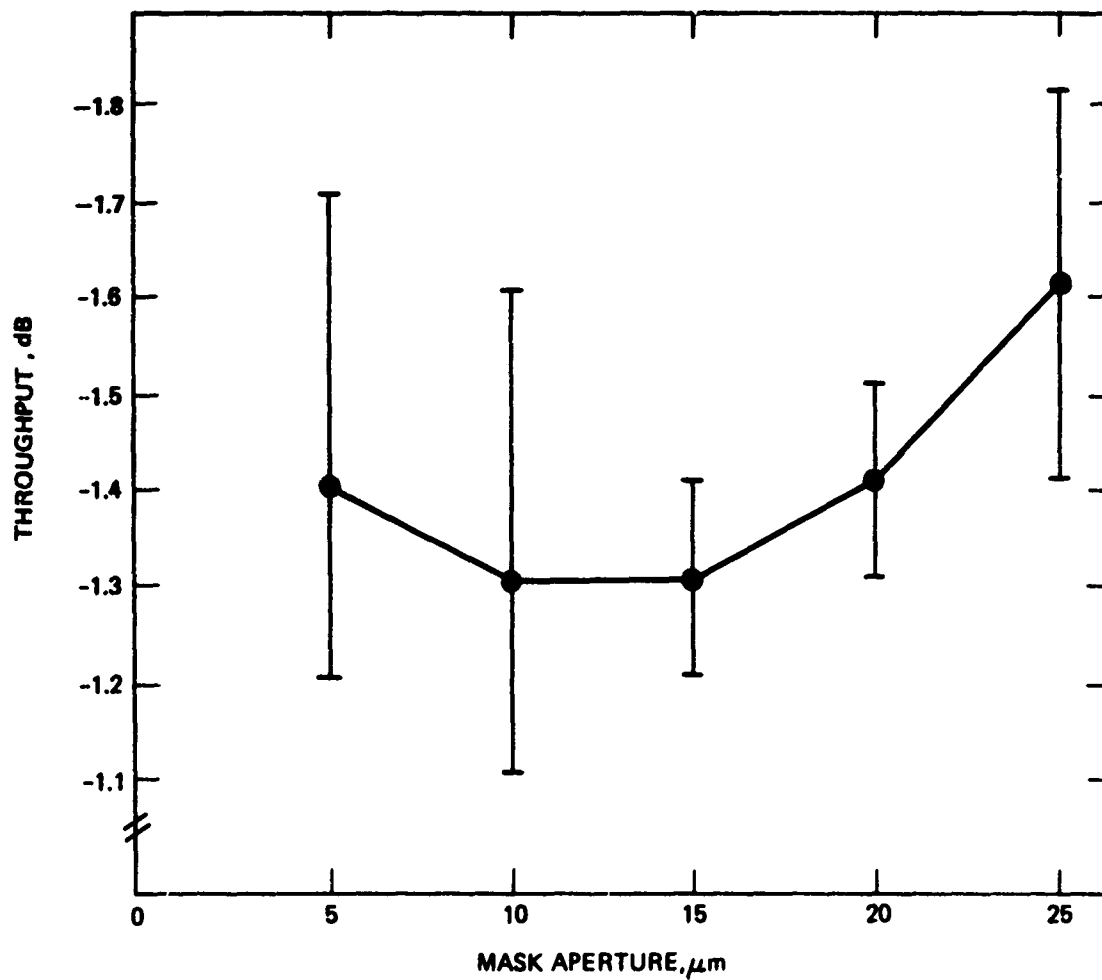
Figure 15. Throughput results for Ag exchange channel guides versus channel width with step index fibers (NA = 0.2). The average point and the variation of 10 samples are shown.

32

D. THROUGHPUT RESULTS FOR BURIED CHANNEL GUIDES

The buried channel guides formed by double exchange (Ag/Na) were recently measured. Very clear differences in the propagation characteristics were observed for buried guides compared to unburied guides. The absence of surface scattering in almost every sample is quite impressive. No bright scattering sites are seen.

The throughput results are shown in Figure 16. Two very interesting points can be made. There is definitely less variation in the data, which supports our contention that surface scattering dominates our results for unburied guides. The throughput loss results do not show a minimum in loss within the range of the mask openings studied. Clearly, the first attempt at the optimization process has not found the best parameter values. The results are, however, quite impressive. The loss is -0.9 to -1.1 dB for the best samples.

The coupling losses may be further reduced with careful optimization. Much work must be done to optimize the process fully. The technical questions that need to be addressed are

- Does the incomplete burying affect the throughput?

- Where is the dominant coupling loss (input or output)?

- What are the differences between step- and graded-index fiber results?

- What are the optimum conditions and the lowest loss possible?

Optimization of the coupling should be the major emphasis of a subsequent program. We feel that a goal of -0.5 dB throughput loss in the 0.85- to 1.30-μm range for step-index fiber is a reasonable objective.

-1.5

-1.0

THROUGHPUT , dB

THROUGHPUT/MASK APERTURE
SAMPLE NO. 60
P6 90 = K1130

0   5   10   15   20   25

MASK APERTURE, μm
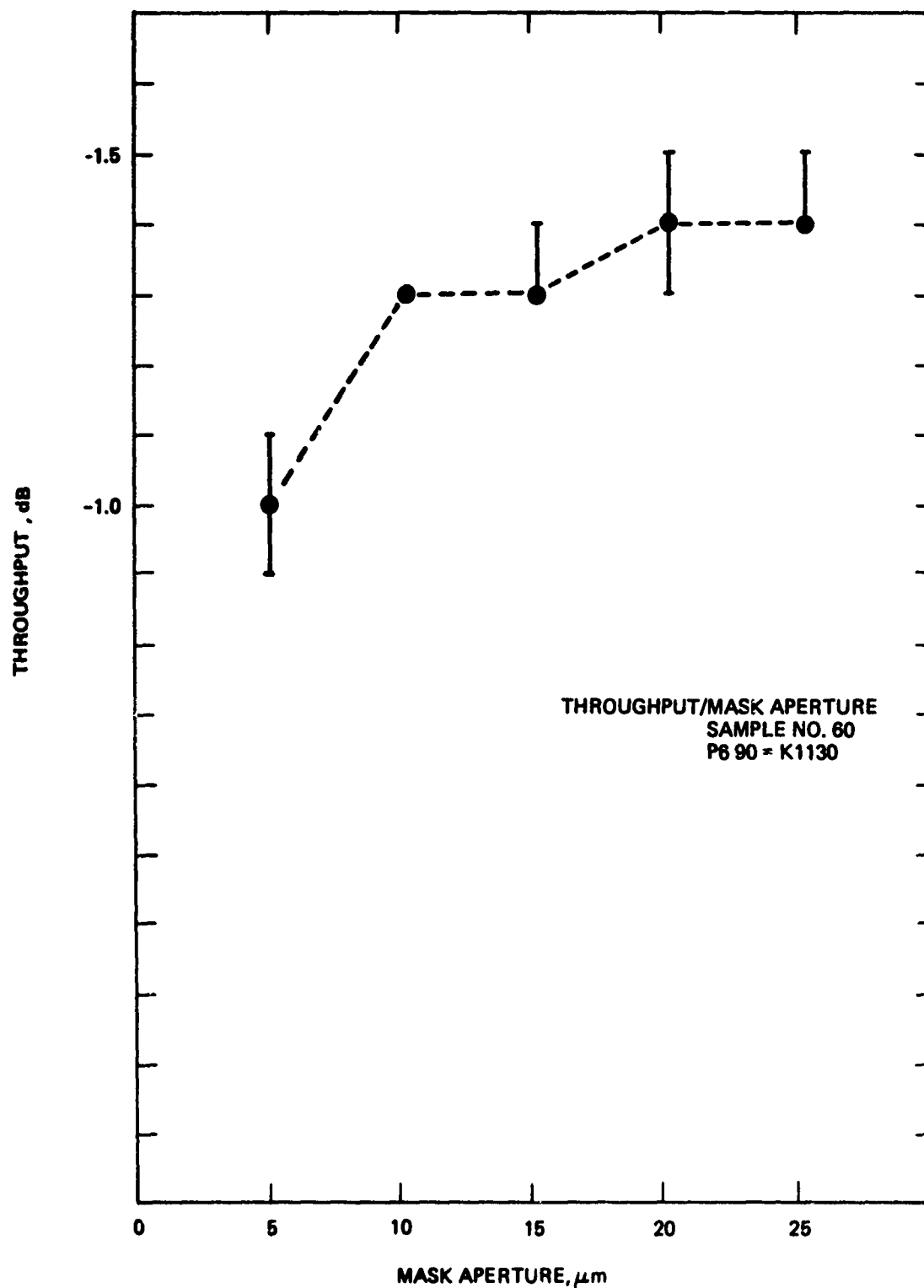
Figure 16.   Throughput results for Ag/Na exchange channel guides with
step index fibers (NA = 0.2).   The ¢ tent of variation for
these samples is smaller than for unburied guies.

SECTION 4

DEVICE DESIGN

A.   PLANAR COUPLERS — STAR DESIGN

This section describes a ray tracing investigation of the multimode planar star coupler[11] illustrated in Figure 17. Ray input is from the left into one of the high-index channel guides of width $2X_B$. The input separation between these high-index regions is $2X_T$. The input and output channel regions are connected by an input horn structure, a mixing region of length Z, and an output horn structure. The length of the horn structure is determined by X_T and the angle θ. All high-index regions have a depth of $2Y_B$. This investigation was made to characterize the partitioning of light into the planar branches as a function of index profile, device dimensions, and configuration; the losses are also tabulated. Computer ray tracing has been used to identify the important design parameters for the planar star. In the actual devices, the dimensions X_B and Y_B correspond to highly multimode guides (500 to 100 μm). Hence, diffraction effects are negligible, and the results of the ray trace analysis are accurate (i.e., diffraction effects are negligible). Example parameters are the required mixing length for equal partitioning of light into each channel and the horn angle required to reduce significantly the packing fraction losses. It should be pointed out that straight-line ray
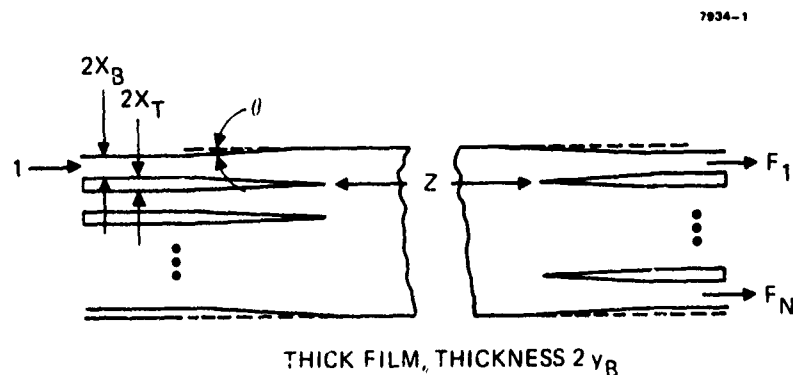
Figure 17.   Schematic of a planar star coupler.

35

tracing requires that the planar guides and the substrate be uniform in refractive index. The ray tracing analysis is limited to such planar structures.

B.   RAY TRACING PROCEDURE

To model the devices accurately, the rays must statistically simulate the total of the modes in the guides. Since the structure that is analyzed is a step-index configuration, we elected to choose the rays randomly so that the angular extent of the numerical aperture is filled uniformly. Although it is also possible to choose randomly the initial x and y position of the rays in some z plane, we elected a single ray from the center of each rectangle. Using this algorithm and starting the random number generator at different positions do not affect the final result significantly (<1% variation) if a large number (>5000) of rays are traced. That is, some average properties associated with the motion of a large number of identical systems differing over a range of initial conditions are obtained.

Given the initial values for position (x,y) and direction cosines (k,l,m) of a ray at some z_o(=0), it is possible, in general, to solve for its position and direction cosines at any other value of z.

Snell's law describes the refraction of light through an interface (Figure 17) and is given by

$$n_2\hat{S}_2 \times \hat{G} = n_1\hat{S}_1 \times \hat{G} \tag{4}$$

or

$$(n_2\hat{S}_2 - n_1\hat{S}_1) \times \hat{G} = 0 \quad , \tag{5}$$

where $\hat{S}_1$ is a unit vector in the direction of the ray impinging on the interface, $\hat{G}$ is a unit vector in the direction of the local normal to the interface, n_1 and n_2 are the refractive indices

on the two sides of the interface, and $\hat{S}_2$ is a unit vector in the direction of the ray after refraction and/or reflection ($n_1 = n_2$) at the interface.

Equation 5 is a simple vector relation that can be solved exactly; it is satisfied if the vector in parentheses is collinear with $\overline{G}$, thus allowing one to write

$$n_2\hat{S}_2 - n_1\hat{S}_1 = \Gamma\hat{G} \tag{6}$$

or

$$N_2\hat{S}_2 = n_1\hat{S}_1 - \Gamma\hat{G} \;, \tag{7}$$

where Γ is yet an unknown quantity. The dot product of Equation 7 with itself eliminates the unknown $\hat{S}_2$ and gives the following quadratic equations in Γ:

$$\Gamma^2 - 2\Gamma(n_1\hat{S}_1 \cdot \hat{G}) + (n_1^2 - n_2^2) = 0 \tag{8}$$

or

$$\Gamma = (n_1\overline{S}_1 \cdot \overline{G}) \pm \left[(n_1\hat{S}_1 \cdot \hat{G})^2 - n_1^2 + n_2^2 \right]^{1/2} \;. \tag{9}$$

By the appropriate choice of Γ, both refraction and total internal reflection from the refractive interface can be accurately described. If the square root is imaginary, the ray is totally internally reflected, and the positive sign is chosen after setting $n_1 = n_2$:

$$\hat{S}_2 = \hat{S}_1 - (2\hat{S}_1 \cdot \hat{G})\hat{G}. \tag{10}$$

37

If the square root is real, the smaller absolute value of Γ gives the $\hat{S}_2$ corresponding to the physical situation of refraction (Figure 18). Substitution of this value for Γ into Equation 7 gives the new ray direction $\hat{S}_2$. In the analysis of the planar star, rays of this sort are lost from the device and thus summed to evaluate the losses.

The algorithms for ray tracing through a device are listed below, with further detail given in the next section:

(1) Initialize ray

(2) Determine surface of intersection

(3) Apply Equation 10 if square root in Equation 9 is imaginary; if square root is real, sum the ray as lost and go to (1)

(4) Repeat (2) and (3) until ray exits device

(5) Sum ray as exiting appropriate port and go to (1).

The parameters of interest for star design are (Figure 17):

θ = half angle to taper angle

X_T = halfwidth of wall

X_B = halfwidth of channel

Y_B = half thickness of film

Z = mixing length

N = number of ports, numerical aperture of the guide, and index of the surrounding region.

C.   CALCULATION ALGORITHM

In the above algorithm, the ray intersections with the guide boundaries remain to be defined. There are five independent sections (input guides, output guides, input horns, output horns, and mixing region) of the planar star. Each has to be handled separately with the appropriate coordinate transformation between regions. The coordinate system for
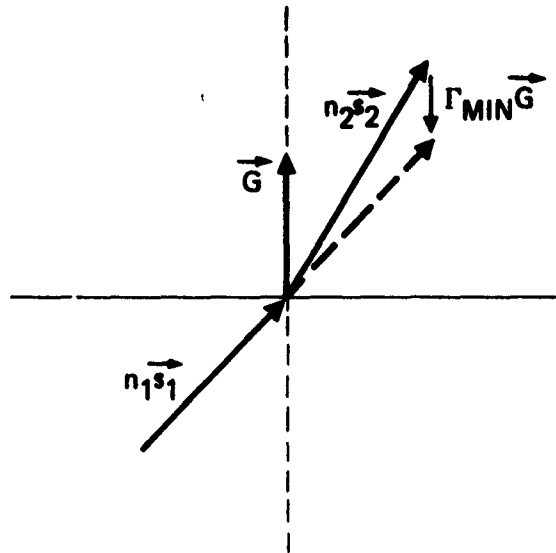
(a)
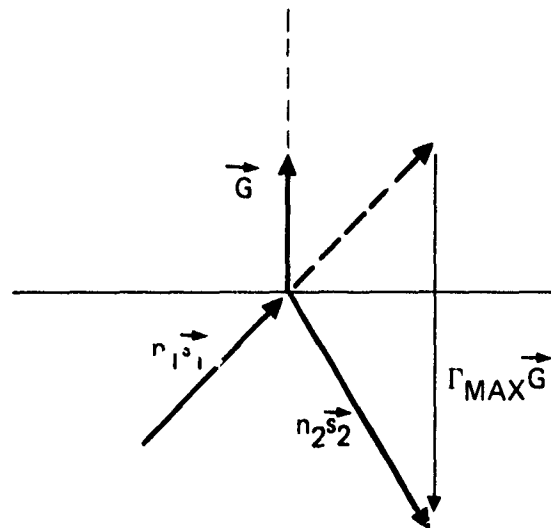
(b)

Figure 18.   Illustration showing the
appropriate choice of Γ
in the solution of Snell's
law is Γ_{min}.

39

each individual guide (horn, mixing region, etc.) is a z axis, which bisects the guide with transverse x and y axes. The x axis is parallel to the plane of the substrate.

Let the ray position be given by

$$\bar{P} = x\bar{i} + y\bar{j} + z\bar{k} \tag{11}$$

and by the ray direction of

$$\bar{S} = l\bar{i} + m\bar{j} + n\bar{k}. \tag{12}$$

If we are in any of the three uniform regions (input guide, output guide, or mixing region), the next boundary intersection $\bar{P}_I$ is given by

$$\bar{P}_I = \bar{P} + \bar{S}D, \tag{13}$$

where D is the smallest of the following three distances:

● The distance to the x plane

$$DX = (x - lS_G/|l|)/l \tag{14}$$

● The distance to the y plane

$$DY = (y - mY_G/|m|)/m \tag{15}$$

● The distance to the end of the guide

$$DZ = (z - z_{max})/n, \tag{16}$$

where $2X_G$, $2Y_G$, and z_{max} are the guide dimensions. For example, in the mixing region

$$N_G = (X_B + S_T)N \tag{17}$$

$$Y_G + Y_B \tag{18}$$

$$z_{max} + Z. \tag{19}$$

In the horns, the next boundary intersection (Equation 12) is given by $z_{max} = X_T/\tan\theta$, the shortest distance between the y plane (Equation 14) and the end of the horn (Equation 15), or one of the two horn boundaries:

$$D = \frac{X - (M2 + B)}{Mn - 1} , \tag{20}$$

where

$$M = \pm\tan \tag{21}$$

$$N = \pm X_B \tag{22}$$

for the input horns and

$$M = \pm\tan(-\theta) , \tag{23}$$

$$B = \pm(S_B + X_T) \tag{24}$$

for the output horns.

41

D. RAY TRACE ANALYSIS

In the ray trace program, rays can be input at any of the N ports; the program outputs are the number of rays that exit each port and the number of rays that are lost. Figure 19 shows the result of varying the mixing length Z for an eight-port star coupler; each line represents the number of rays that exit a given port. The number of rays to each of the ports with ports 1-4 for input and Z/X_B = 2750 are given in Table 1. The number of rays lost or not satisfying the condition for total internal reflection at any one of the guide wall intersections is also given in Table 1. A total of 10,000 rays were traced for each input.

The major loss in conventional star couplers is the packing fraction loss. The purpose of the horn structure in the planar star coupler is to provide a means to reduce this loss. The losses for an eight-port
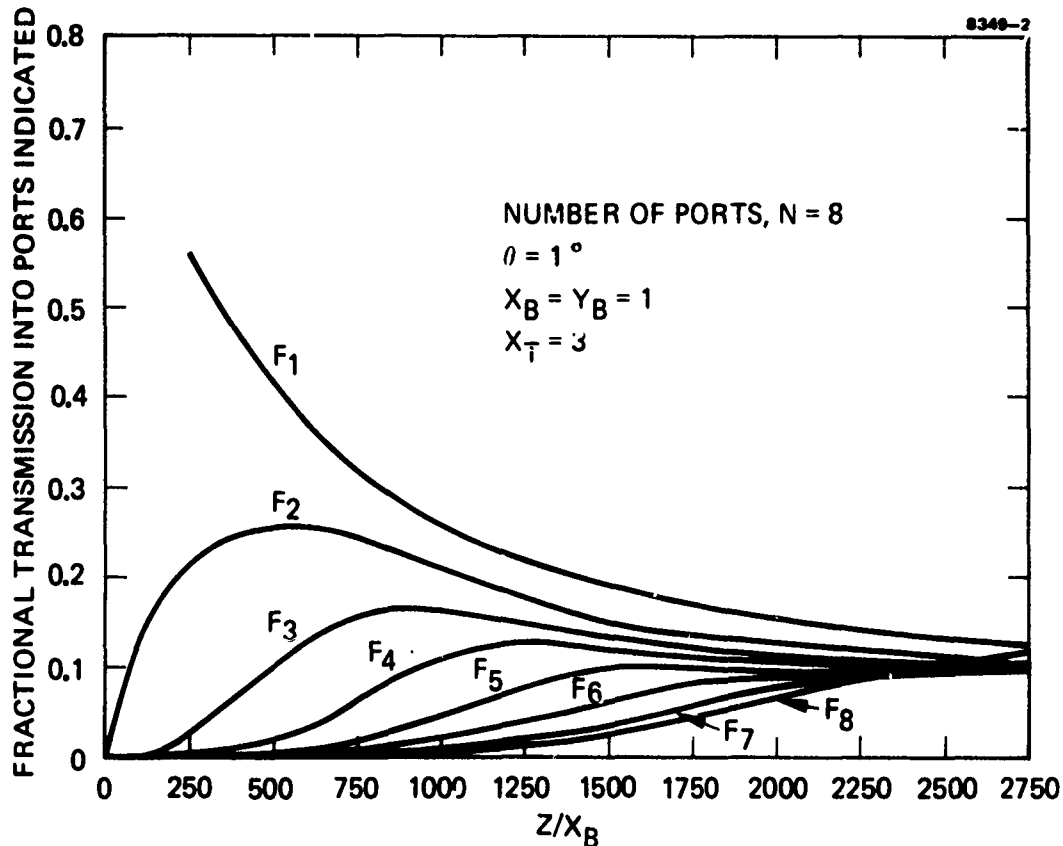
Figure 19. Fractional transmission of an eight-port star coupler versus mixing length.

42

Table 1. Number of Rays to Each Port

Input Port	Output Port			
	1	2	3	4
1	1,195	999	927	905
2	967	942	922	957
3	948	934	964	1,065
4	952	1,014	1,072	1,053
5	891	967	1,084	1,077
6	966	991	992	1,082
7	1,020	988	1,002	918
8	1,162	1,107	997	884
Loss	1,999	2,058	2,040	2,059
Total	10,000	10,000	10,000	10,000

star have been calculated with the horn angle θ as a variable. The result of this calculation is shown in Figure 20. For a horn angle equal to or greater than half of the numerical aperture (NA/2) of the guide, the loss is equal to the structure packing fraction. In this case, the loss is

$$X_T / (X_T + X_B) = 0.75. \tag{25}$$

At reduced angles, the loss is substantially reduced. The packing fraction loss for horn angles larger than NA/2 can be easily understood. Any ray that strikes the horn boundaries will have its direction changed by an angle equal to twice the horn angle. Hence, for any horn angle

43
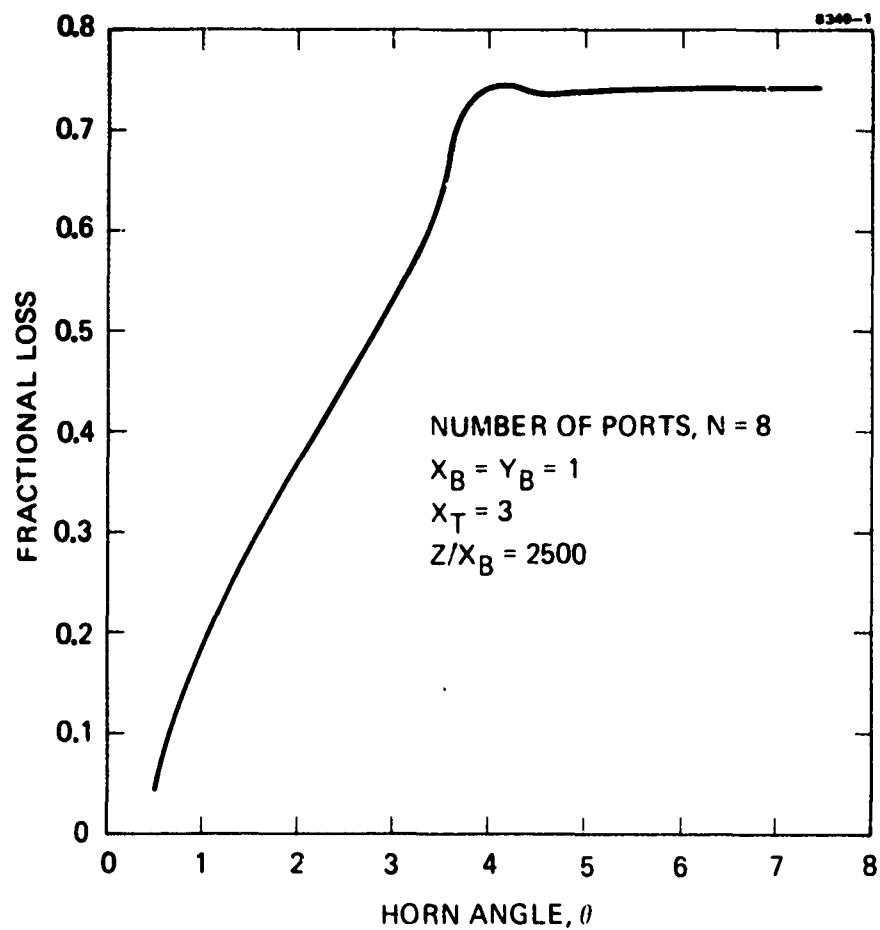
Figure 20. Fractional loss of an eight-port star versus horn angle θ. A loss of 75% is the structural packing fraction.

larger than NA/2, the ray angle after striking the horn will be larger than the guide NA and will be lost. Reduced horn angles result in an adiabatic transition and reduced loss.

In conclusion, the planar star coupler design presented shows that the packing fraction loss of the planar star coupler can be decreased. This is achieved by tapering the input guides with a taper angle less than half of the NA of the guide. The length of the mixing region can be chosen for equal coupling to all ports.

E.   PLANAR Y COUPLER DESIGN

The planar Y coupler configuration which has been studied is shown in Figure 21. The inputs to the program are X_B, X, y_B, the numerical aperture of the guide, the index of the surrounding region, and the input port. Using x as a parameter and θ as a variable, Figure 22 shows the transmission properties (port 1 to port 2) of this device. Figure 23 shows the fractional transmission from port 3 to port 1. Figure 24 shows the fractional transmission from port 2 to port 1. Further analysis will be performed to understand the variations in the low angle region of these plots.

The program has been expanded to determine the angular extent of the light coupled from one branch to the other, and far field spot diagrams have been generated. The loss of coupling the square guide to a circular fiber has also been investigated. It should be emphasized that all results presented in this section were calculated.

7846-4

THICK FILM OF
THICKNESS OF $2Y_B$

$2X_B$

$2X$

θ

① ② ③
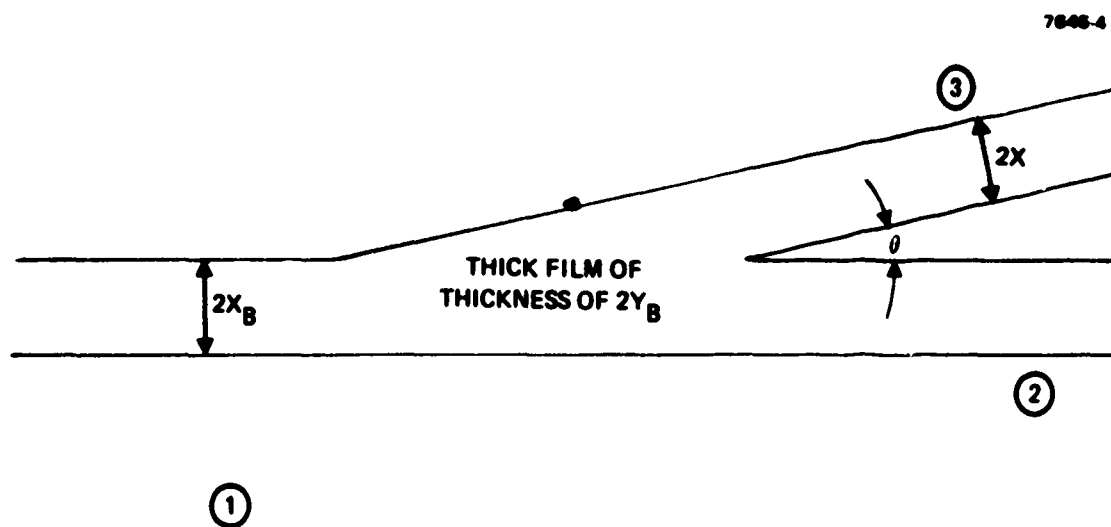
Figure 21. Schematic of the planar Y coupler.

Figure 22. Fractional transmission from port 1 to 2 for a
Y coupler versus coupling angle.

47

Figure 23. Fractional transmission from port 3 to 1 for the planar
Y coupler versus the coupling angle. The width x is
used as a parameter.

48

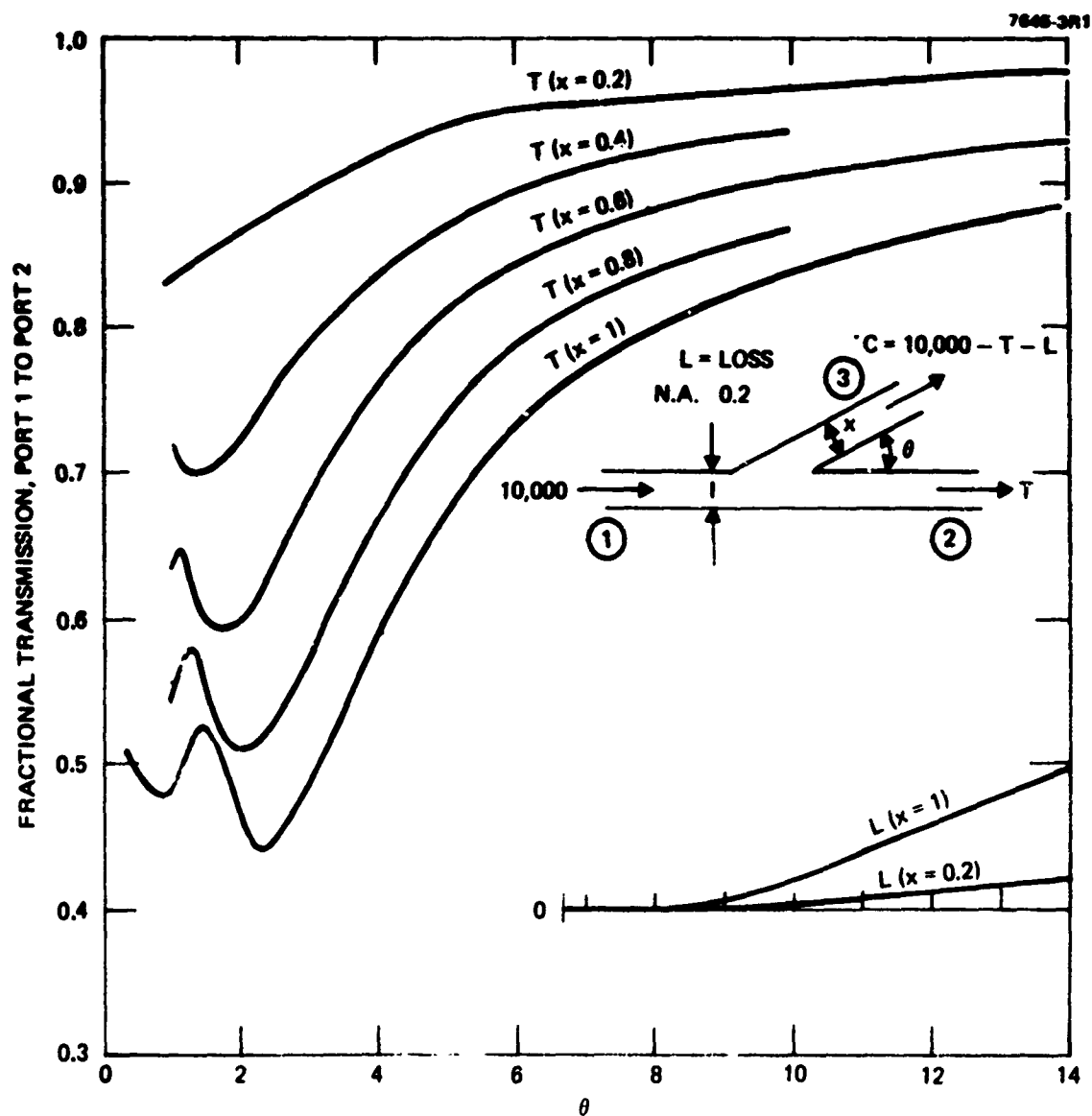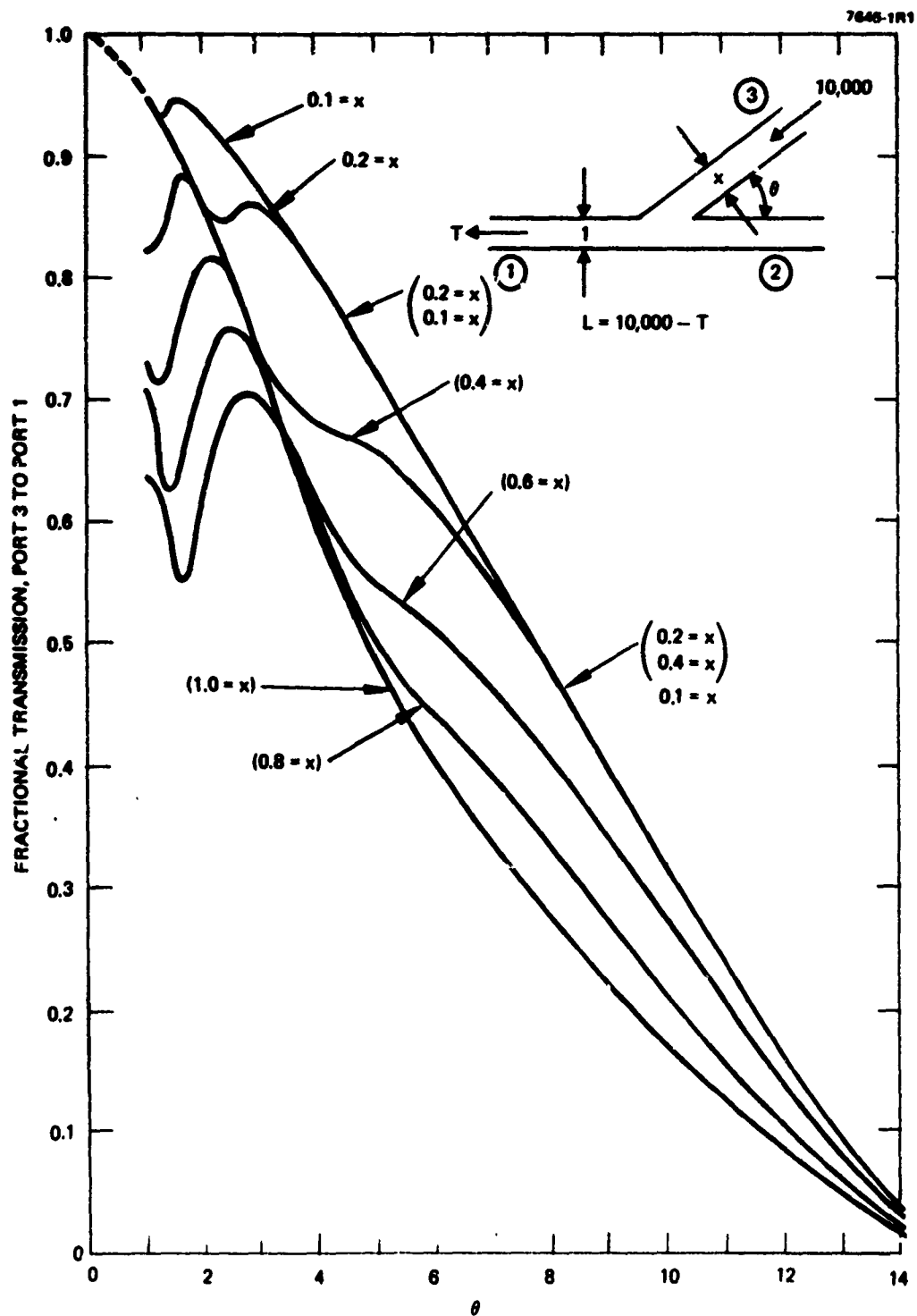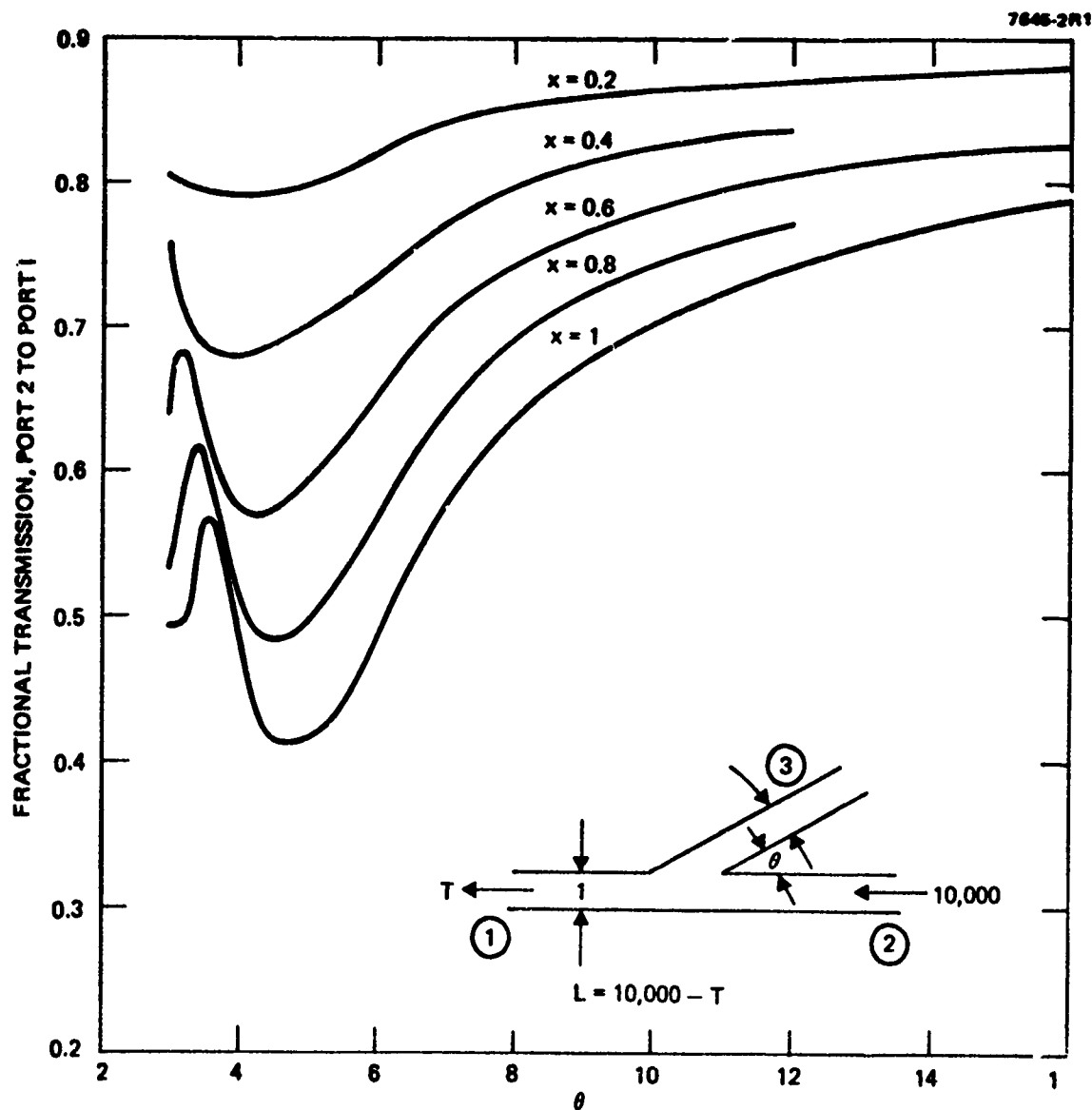Figure 24. Fractional transmission from port 2 to 1 for the planar Y coupler versus the coupling angle. The width x of the branch is used as a parameter.

49

SECTION 5

COUPLER FABRICATION AND OPTIMIZATION

Planar couplers were fabricated and tested during this program. The coupler effort was initiated to demonstrate the total process of ion exchange guide formation, fiber interfacing, and testing. The experience gained by fabricating these devices is quite extensive. The reviews presented here describe splitter development and star coupler development.

A. PLANAR SPLITTER DEVELOPMENT

The first devices studied with the planar processing were planar splitters. The results clearly demonstrated the batch processing potential of planar couplers. They also highlighted the major problem with the planar approach — coupling the fibers to the channel guides.

The guides were processed by the Li_2SO_4-K_2SO_4 guide formation techniques described above.

Figure 25 shows a top view of an ion exchange slide with coupling structures formed using 1, 2, 3, 4, and 5° branches. The coupling branches are continued parallel to the main branch when 300-μm separation is attained. This facilitates the power measurement because the optical fibers placed at the output ports may be perpendicular to the slide end face. The output of the 1° branch is also shown in Figure 25. Using graded-index fibers (Corning) of 65 μm core size, the coupling ratios were measured from the fiber input to fiber output with the planar coupler in between. Mode strippers were used to ensure that only guided modes were measured. The results are shown in Figure 26, where, for two outputs P_1 and P_0, we have graphed $P_1/(P_1 + P_0)$, where P_1 is the branch output, and P_0 is the straight output. A clear trend of decreasing coupling with increased branching angle is observed. The error bars are due mainly to the experimental difficulties in fiber placement precision and processing variations. To demonstrate further

51

5°
4°
3°
2°
1°

300 μm SPACING
BETWEEN
GUIDES
(75 μm WIDE)
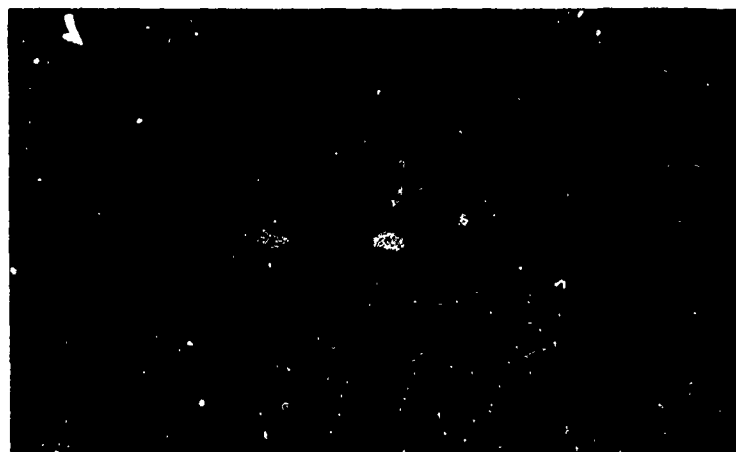
OUTPUTS OF 1° COUPLER
(300 μm CENTER TO CENTER)

Figure 25. Planar coupler array formed by ion exchange in
a glass slide.
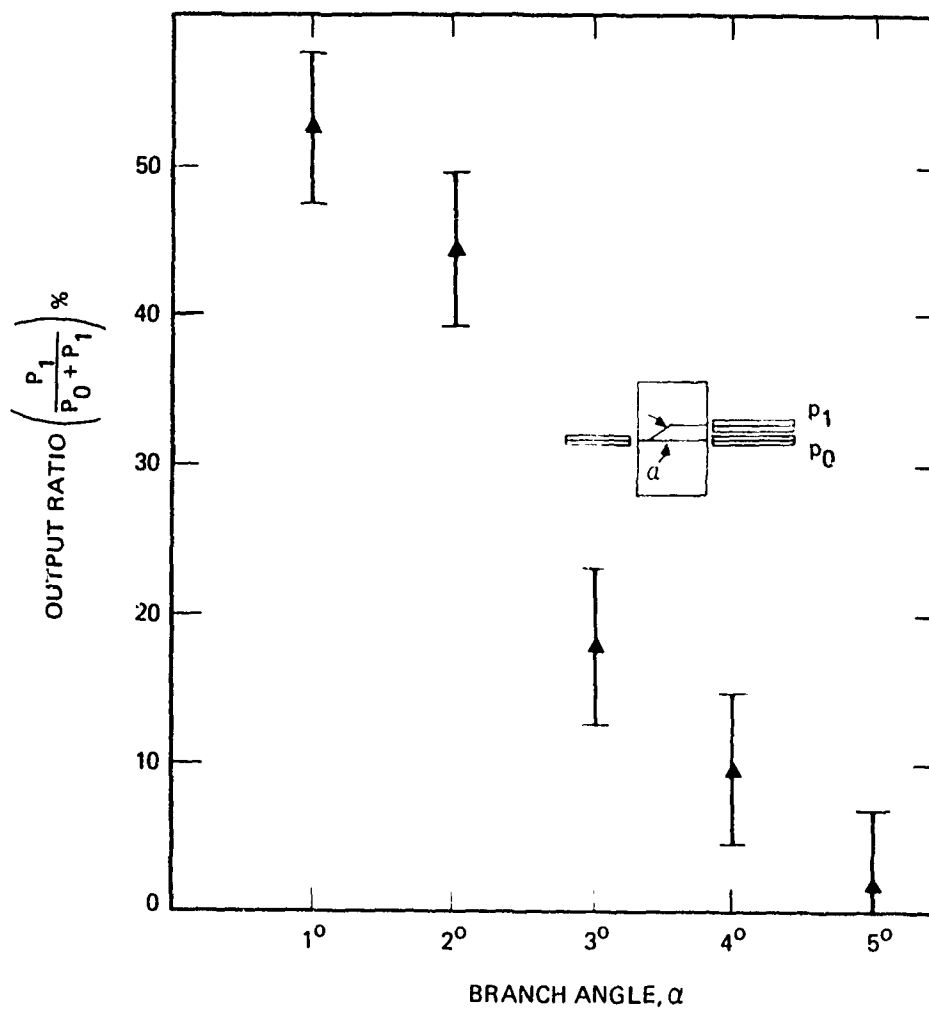
Figure 26. Coupling ratio results for different branch angles.

the versatility of the planar coupler approach, the tapered coupler structure shown in Figure 27 has been formed. The coupling is controlled by varying the parameters d_2, θ_1, θ_2, and θ_3. For $d_1 = 75$, $d_2 = 50$, $d_3 = 100$ μm, $\theta_1 = 2^{\circ}$, $\theta_2 = 0.66^{\circ}$, and $\theta_3 = 1^{\circ}$, a coupler with a 20:1 tap ratio was measured.

The ion exchange process seems well suited for fiber optic coupler applications; in fact, the guide losses we have observed are quite low. We estimate that the guide losses are 0.1 to 0.5 dB/cm depending on processing variations. The dominant scattering mechanism is due to surface cracks, which have been largely eliminated by preprocessing the slide. The crack density is reduced by a process involving a 5 min etching of the slide in 5% aqueous HF. In addition, a fire polishing of the slides prior to ion exchange reduces the final crack density.

B.   PLANAR STAR COUPLER DEVELOPMENT

We have designed planar star devices using the ray-tracing computer program. In contrast to conventional star designs in which a simple

7445-1
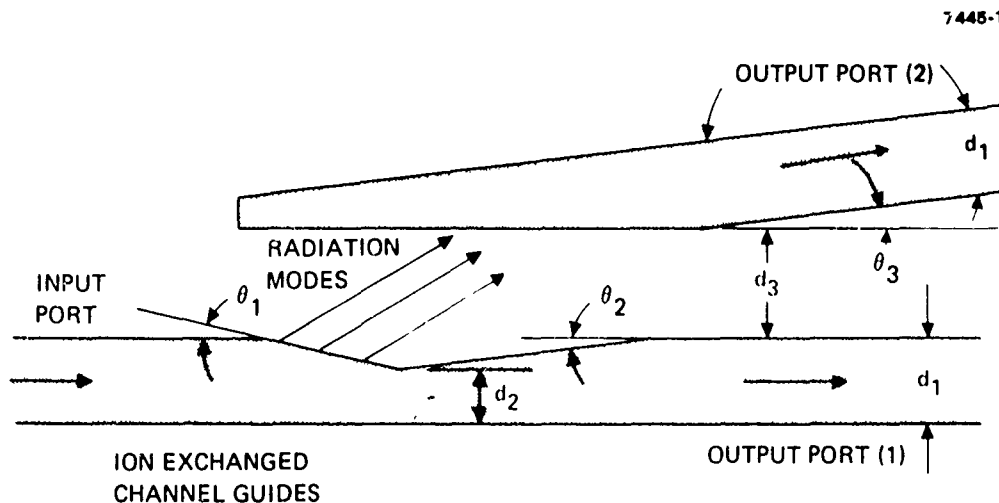
Figure 27. Tapered coupler of planar variety formed by ion exchange. Coupling is due to radiation excitation by the taper.

mixing region is formed, our planar design utilizes horns to form a
transition from the channel guides to the planar mixing region. This
is shown in Figure 28 for a reflective star. The computer design param-
eters are taper angle, channel width, interchannel spacing, mixing
length for a given number of ports, and guide numerical aperture. An
example for our analysis is the fractional transmission for an 8-port
star with channel guides of width $2X_B$ and channel spacing of $6X_B$, shown
in Figure 19. This calculation shows that, as the mixing length Z is
increased (with the taper angle $\theta = 1^{o}$), the output destiny distribution
is partitioned equally into the output channels. The fractional power
loss of the structure is 0.2. This represents an improvement over the
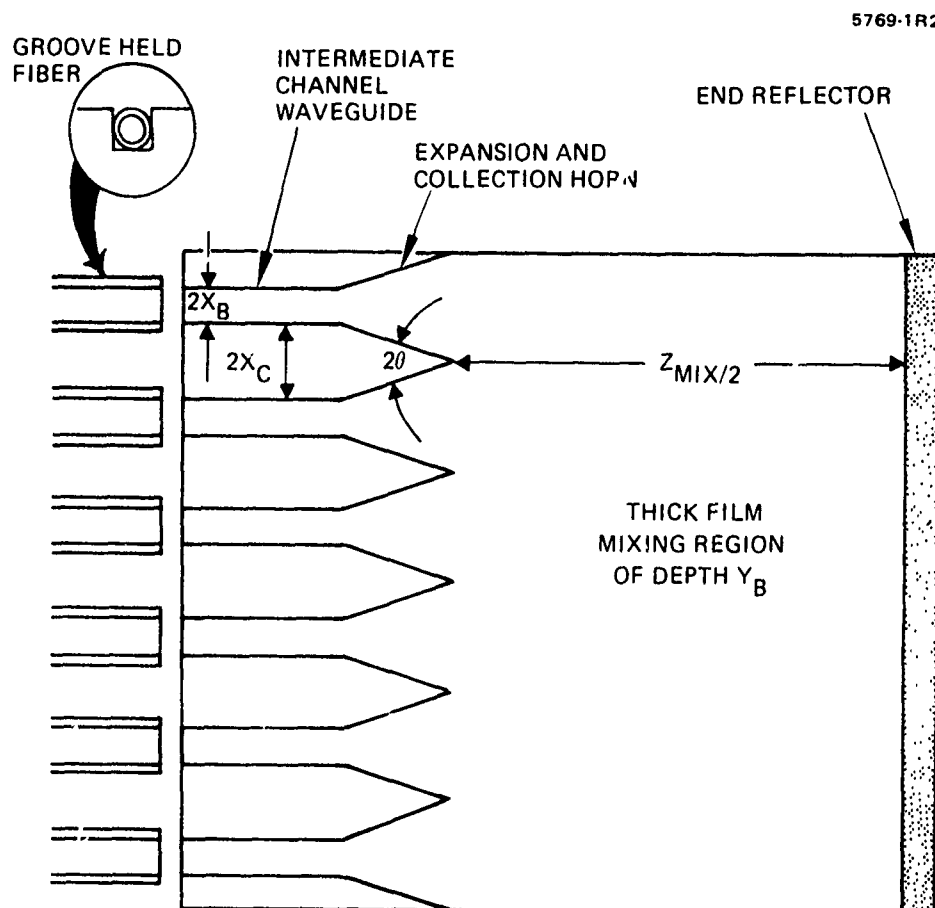
Figure 28. Reflection star-coupler design using a horn
transition to the mixing region.

simple packing fraction losses of ∿0.25 for a linear array of 8 fibers
(with core diameter equal to one half of the total fiber diameter)
coupled to a planar mixing rod of thickness equal to the core diameter.
It is worth noting that, for conventional 7-port stars based on a
hexagonal array, the packing fraction loss is 0.72. This improvement
is attained as long as the taper angle is less than the numerical aper-
ture of the guide. The mixing lengths are increased over a conventional
mixing rod because of the collimating effect of the horn.

An 8-port star coupler device was fabricated using the ion exchange
process. The output of a transmission star when excited at one of the
ports by a graded-index fiber (Corning) is shown in Figure 29.

The measured throughput matrices of a transmission star coupler
with 8 input fibers and 8 output fibers cemented in place are given
here. Plates containing the stars were immersed in the Li_2SO_4-K_2SO_4

CENTER TO CENTER DISTANCE = 241 μm   8399-12
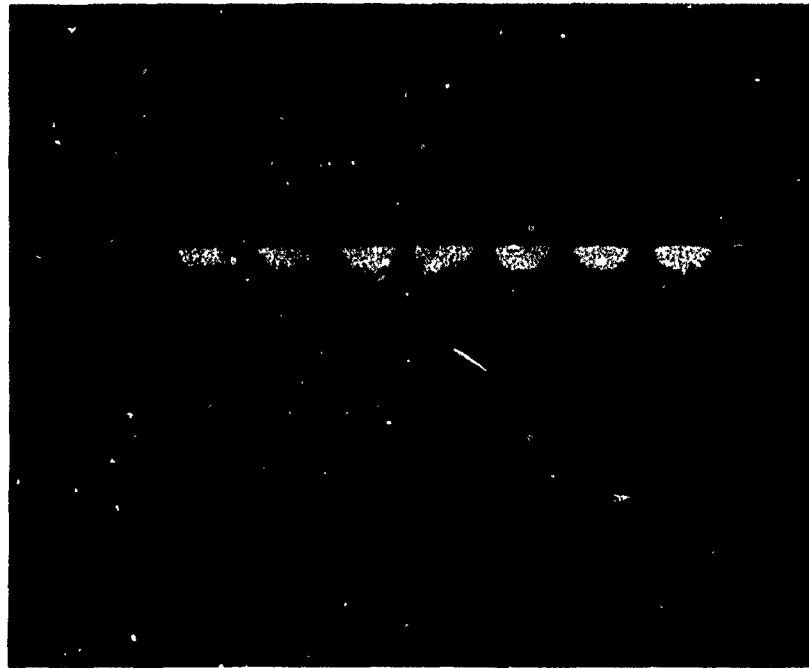
Figure 29. Output of an 8-port star coupler.

melt for the following temperatures and time intervals: 605°C, 5 min; 605°C, 10 min; 605°C, 15 min; 585°C, 20 min; 585°C, 40 min. Two stars were located on each plate. The plate immersed for 20 min at 585°C appeared to yield the best stars. A fairly clean near-field output pattern is observed when light from a fiber is inputted into any of the entrance ports. With light from a fiber (~200 µW) inputted into any of the entrance ports, the maximum sum total power intercepted by a fiber was 24 µW (-9.2 dB).

There were considerable variations in the outputs of the eight exit ports, varying at most by a factor of three. The variations may be due to imperfection scattering, graded index structure boundaries, and/or lack of sufficient mixing lengths for the graded index structure. The cause of these variations will be investigated in the proposed program. We will determine the degree to which our structures reproduce the theoretical design criteria. Star devices made with the higher NA guides formed by Ag ion exchange will be used.

C. STAR COUPLER PERFORMANCE

We attached an eight-fiber ribbon to each end of a transmission star (ion exchange process, 585°C for 20 min) with epoxy as described previously. During the attachment process, while the epoxy was still liquid, we have observed an increase in the throughput to as much as 27 µW (-8.5 dB). Part of this increase can be assigned to the elimination of the air gap; as the epoxy hardens, however, a slight decrease (~5 to 10%) of throughput power is usually observed. Whether the decrease results from refractive index change of the hardened epoxy or from slight misalignment of the ribbon-to-channel connection as the epoxy hardens is not known at this time.

The 8 by 8 matrices shown in Table 2 represent the distribution of light from each input fiber to each of the output fibers for the ribbon-star-ribbon assembly prior to assembly in a breadboard box. The channels are numbered according to Figure 30. Table 2 shows the initial distribution matrix; Table 3 shows the distribution where the input and output are interchanged. The maximum total throughput of Table 2 is

57

CHANNEL   CHANNEL

1 ─   ─ 8
2 ─   ─ 7
3 ─   ─ 6
4 ─   ─ 5
5 ─   ─ 4
6 ─   ─ 3
7 ─   ─ 2
8 ─   ─ 1
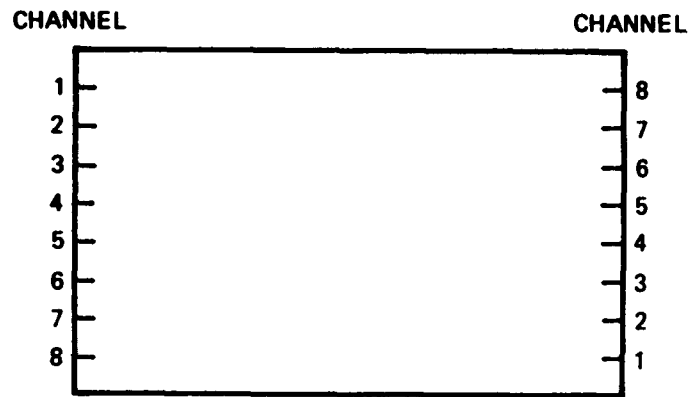
Figure 30.   Numbering of the channels of
the transmission star coupler.

again 24 μm (-9.2 dB), where the power in the input fiber is ∿200 μW.
The average total throughput is 18.1 μW (-10.4 dB). We note that one
of the output channels is much lower than the average distribution,
particularly with input into channels 1 and 8. We do not yet know the
reason for this behavior. It appears that a modification of the outer
boundaries of the star, to compensate for the graded index of the mixing
region, may correct the low output of the channel. More detailed com-
puter studies are expected to clarify the result. This will be done on
the proposed program.

The lower matrix (with interchanged input and output) shows total
outputs lower (∿ -1 to -2 dB) than the upper matrix. At this research
stage, we do not believe that this is significant. The stars were ion
exchanged in a vertical oven with possible thermal gradients in the
melt. Inhomogeneous ion exchange could have resulted. Future work is
expected to show uniform reciprocal distributions as the process is
improved.

The 8x8 distribution matrices of the planar star coupler assembled
in a box with 16 fiber connectors and 16 pigtails were measured and are
given in Table 4; with input and output reversed, they are given in
Table 5. Recall that the matrix in Tables 2 and 3 is that for the star

Table 2. Distribution Matrix For 8x8 Planar Transmission Star #1,
With Two Sets of Fiber Ribbons

Input #1 End	Output #2 End								Total Power, µW
	1	2	3	4	5	6	7	8	
1	2.46	1.60	2.26	1.01	3.78	5.99	5.14	0.57	22.31
2	3.30	3.26	2.48	5.41	1.59	4.05	2.68	1.45	24.22
3	0.60	0.92	1.65	3.22	4.30	2.43	2.33	1.79	17.24
4	0.40	0.46	0.58	0.97	2.72	4.56	3.23	3.49	16.41
5	2.53	1.90	2.02	1.15	1.68	1.80	1.75	2.66	15.49
6	1.70	2.03	1.98	1.12	1.76	1.67	2.46	2.79	15.51
7	6.87	3.06	1.38	1.33	1.20	1.23	0.90	0.97	16.94
8	0.70	6.90	3.05	1.30	1.14	0.93	0.96	1.34	16.32
AVG.									18.1 µW

Table 3. Same as Table 2, Except Input and Output Are Reversed

Input #2 End	Output #1 End								Total Power, µW
	1	2	3	4	5	6	7	8	
1	3.59	2.38	0.85	0.54	1.48	1.24	1.77	0.68	12.55
2	3.29	3.18	0.86	0.69	1.00	1.68	0.85	1.45	13.0
3	3.20	3.61	1.42	0.37	0.52	0.78	0.56	0.67	11.13
4	2.50	4.60	3.25	0.64	0.30	0.51	0.63	0.69	13.12
5	10.70	2.50	1.81	1.38	0.55	0.82	0.40	0.46	18.62
6	3.49	5.00	1.43	1.42	0.72	0.88	0.41	0.36	13.71
7	2.37	2.33	1.49	0.56	1.28	1.75	0.47	0.33	10.58
8	0.35	2.30	0.98	2.78	2.51	1.39	0.72	0.50	11.53
AVG.									13.03

Table 4. Distribution Matrix for Star #1, Breadboarded in a Box, With Fiber Connectors

Input	Output (White Dot End)								Total µW Sum Measurement	
	1	2	3	4	5	6	7	8		
1	1.6	1.3	1.6	1.3	2.5	2.5	2.8	0.50	14.1	14.40
2	1.6	1.5	1.5	3.7	1.1	2.9	1.6	1.0	14.9	15.60
3	0.52	1.1	2.0	3.2	3.2	1.5	1.2	1.2	13.9	13.23
4	0.33	0.33	0.46	0.58	1.8	1.9	1.5	1.8	8.7	8.70
5	1.6	1.3	1.0	0.91	1.3	1.4	1.3	1.8	10.6	10.93
6	1.0	1.1	0.80	0.56	0.91	1.6	0.96	1.6	8.5	9.87
7	2.0	1.7	0.62	0.91	0.60	0.41	0.42	0.45	7.1	7.65
8	0.50	2.7	1.2	0.60	0.77	0.42	0.50	0.80	7.5	8.20
AVG.									10.7	11.1

Table 5. Same as Table 4, Except Input and Output Reversed

Input (White Dot End)	Output								Total µW Sum Measurement	
	1	2	3	4	5	6	7	8		
1	1.6	1.6	0.57	0.36	2.0	0.67	2.0	0.73	9.5	10.36
2	0.85	1.4	0.70	0.26	0.33	0.60	0.54	0.67	5.4	6.50
3	2.1	1.9	1.3	0.42	0.59	0.65	0.22	1.0	8.2	8.93
4	0.72	0.9	1.7	0.26	0.47	0.40	0.32	0.52	6.3	6.42
5	2.7	1.5	2.1	0.81	0.53	0.57	0.24	0.40	8.9	9.45
6	1.2	2.6	0.90	1.2	0.86	0.58	0.22	0.20	7.8	8.50
7	0.93	6.1	6.3	0.90	1.3	0.68	0.15	0.22	6.6	8.20
8	0.13	1.4	0.93	2.3	1.74	0.47	0.38	0.30	7.7	8.02
AVG.									7.6	8.5

with ribbon pigtails and that the matrix in Tables 4 and 5 is that for
the same star plus ribbon, but with eight input and eight output fiber
connectors. The average loss due to the two connectors is ∿2.3 dB per
connector, or a loss of -1.2 dB per connector. Figure 31 shows a
packaged version of the 8-port star coupler with connectors.

The matrix measurements of the boxed star were sensitive to move-
ment of certain of the input pigtails and to launch conditions of the
laser light. Whether this problem arises from distortion at the con-
nector is not yet clear, but the effect will be examined more fully and
corrected.

The highest throughput was down ∿ -9 dB relative to the power in
the input fiber. We can partition the loss as follows:

Measured Insertion Loss	=	Measured Coupling Loss	+	Estimated Propagation Loss	+	Estimated Internal Loss

or

$$9 \text{ dB} = 4.2 \text{ dB} + (0.1 \text{ dB/cm}) (8 \text{ cm}) + (4.0 \text{ dB}) \quad .$$

The measured coupling loss of 4.2 dB was determined from the experi-
ments with parallel channels described previously. The remainder of
the insertion loss is partitioned to propagation loss and the internal
loss of the star structure. If the propagation loss is taken to be
very small (0.1 dB/cm), an estimated internal loss of 4.0 dB remains.
The latter loss may be compared with the packing fraction loss of
3.8 dB for a linear array of fiber. We expect that the fiber to star
coupling loss can be reduced to < 1 dB. This could result in an inser-
tion loss of ∿5 to 6 dB. Already, < 1 dB coupling efficiencies have
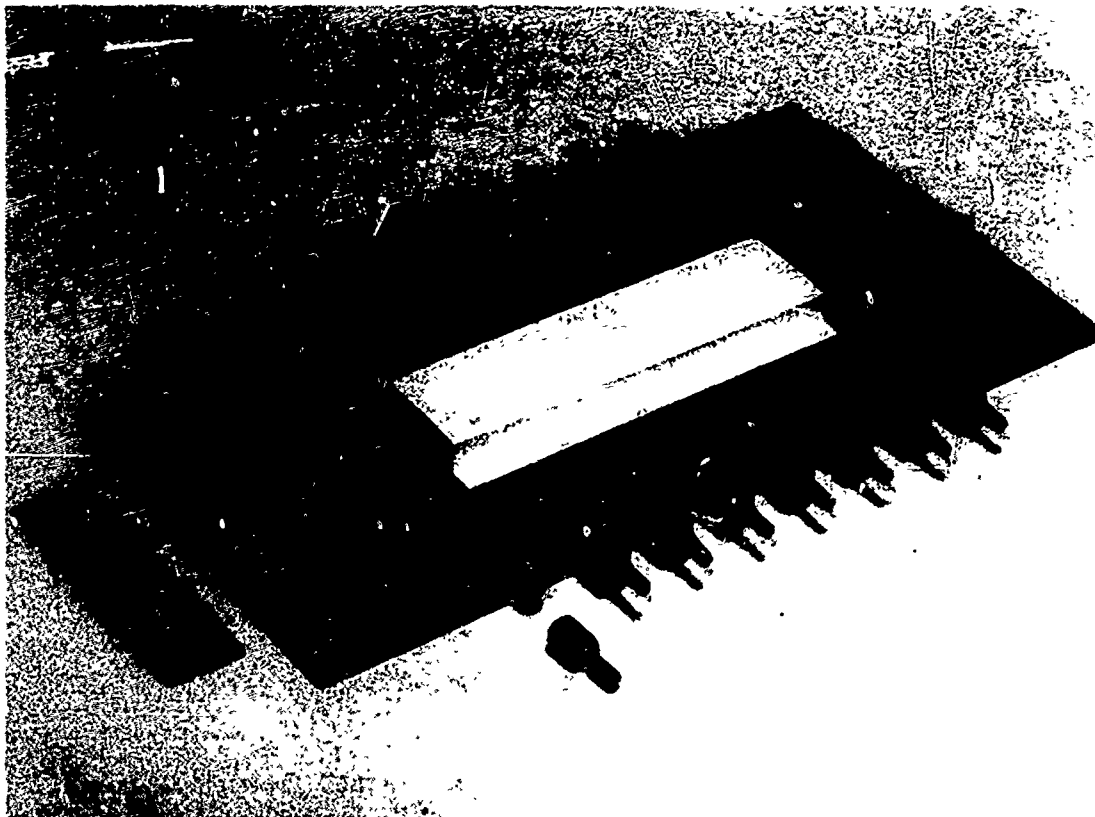been demonstrated (as described above).

61

Figure 31. Star coupler (8 port) assembled and packaged with HAC connectors.

D. FIBER INTERFACING

Photographs of the fiber h⌐ ⌐rs are given in Figures 32 and 33. Conventional silicon selective etching was used to fabricate these holders. The experience gained by these experiments adds to the confidence level we have in this approach to fiber interfacing. The precision control of photolithography is now applicable to both guide formation and fiber holder arrays. We are certain that optimum coupling conditions can be attained by this approach.

9012-9

8 FIBER RIBBON

ETCHED
SILICON

PLANAR GUIDE
SUBSTRATE

UPPER SECTION,
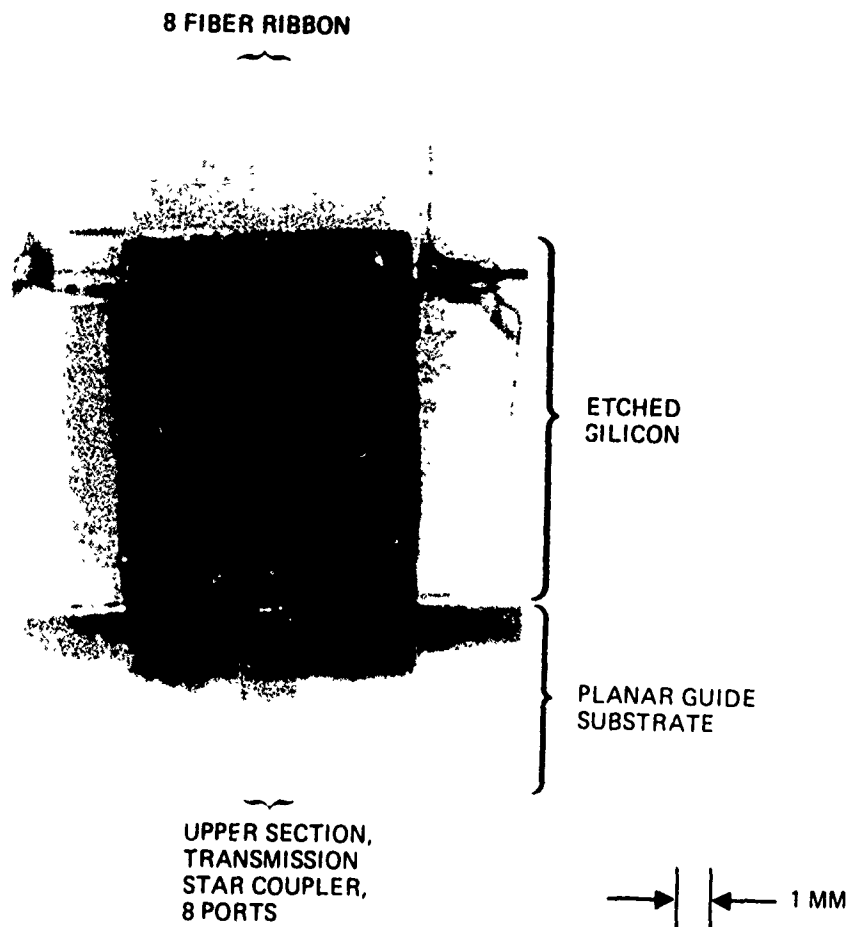TRANSMISSION
STAR COUPLER,
8 PORTS

1 MM

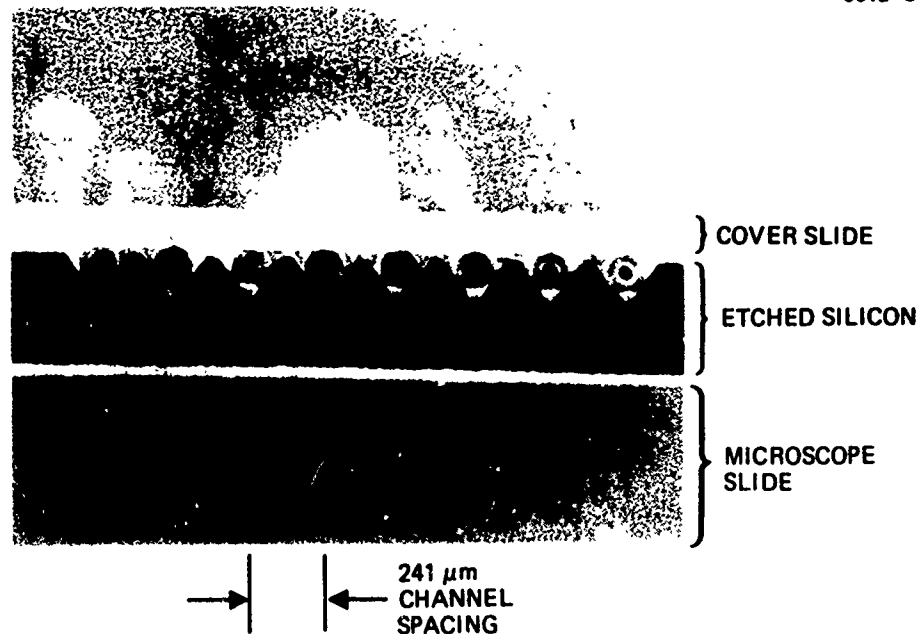Figure 32. Top view of 8 fiber ribbon epoxied to an
8 port transmission star coupler.

Figure 33. End view of 8 fiber ribbon epoxied into etched silicon spacers.

E. Y COUPLERS FORMED BY Ag ION EXCHANGE AND DOUBLE EXCHANGE (Ag/Na)

We recently fabricated optical couplers with the Ag ion exchange and double exchange with Ag and Na. The coupler mask is similar to those described earlier in this section, the only difference is the mask width of 30 μm. The new results arise from an attempt to use the high throughput parameters for forming the coupling structures. The parameters were

Unburied — 300°C, 15 min, 150 V/mm

Buried — 300°C, 7.5 min, 150 V/mm; Na burying

— 400°C, 10 min, 150 V/mm.

The ends of the 1° Y-coupler structures for both the unburied and buried structures are shown in Figure 34. The difference between the
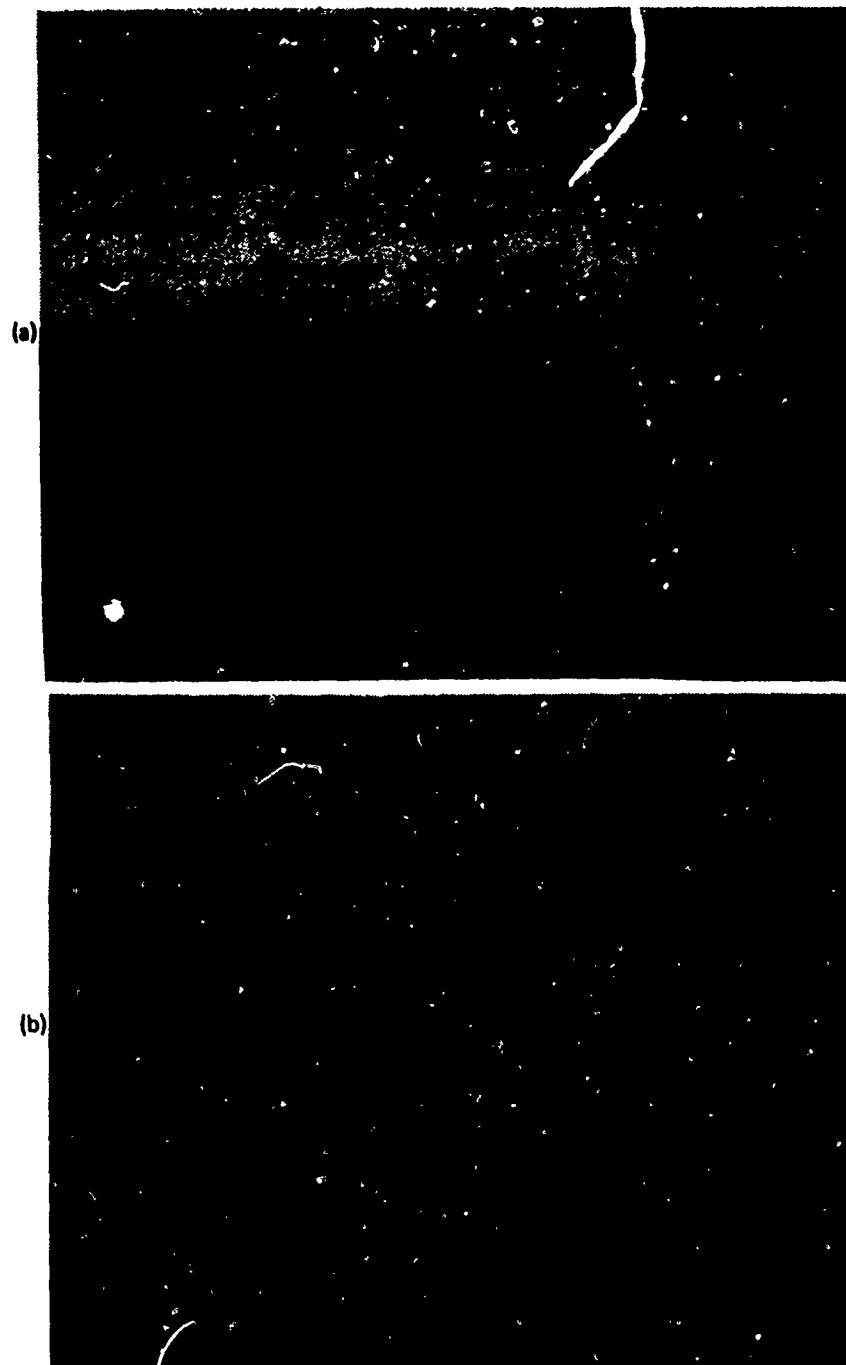
64

Figure 34. End view of the 1° Y-coupler guides:
(a) unburied and (b) buried.

index profile is evident from the guiding of the microscope illumination. The mask utilized had 1, 2, 3, 4, and 5° angle couplers. The total sample length was 1.2 cm.

Measurements of the throughput (F/C/F) were made with HeNe laser light and step index fibers. The output of the buried waveguide structure (1° coupler) is shown in Figure 35. The coupling ratio was 3 dB, as expected. The measured throughput losses for both structures were

Unburied coupler: -3.0 dB

Buried coupler: -2.5 dB .

These insertion losses are low and are in fact state-of-the-art results. However, because of the nonoptimum match with the Corning (80 μm) fibers for the parameters chosen, the results are not as good as can be expected. The optimum cross section is 120 x 70 μm, and the

9807-6

BURIED Y COUPLER (1°)

Figure 35. Output of the buried Y coupler ($1°$) when
excited by a fiber.

66

attained result is 100 x 45 μm. With further optimization, they can be reduced even further. Detailed measurements of the insertion loss for the various tap ratios have not been made. These results will be obtained early in the proposed program and will be included in the design analysis for optimized couplers.

The Corning fibers were changed with Hughes smaller core fibers (50 μm). These fibers were step index (NA = 0.22). The results show a definite improvement. The 1° coupler showed a 1.4 dB loss. This is the best result obtained for planar couplers to date.

SECTION 6

CONCLUSIONS AND RECOMMENDATIONS

Under this contract, the major accomplishments have been in the areas of processing and optical throughput optimization. Specifically, we have:

- Demonstrated field-assisted diffusion of Ag into glass for high-numerical-aperture and step-index guides.

- Demonstrated buried waveguides with double exchange techniques in which Na is re-introduced subsequent to Ag diffusion.

- Demonstrated channel waveguide and coupler formation using masked diffusion.

- Optimized the fiber to channel to fiber coupling by achieving as low as -1 dB throughput loss.

- Demonstrated a 3-dB coupler formed by double-exchange with <2 dB total insertion loss.

These results represent a significant advancement of the state of the art of planar couplers.

Our recommendations for subsequent work are that three areas be emphasized: throughput optimization, coupler fabrication, and evaluation of the devices with LED and laser excitation in the 0.85 to 1.30 μm range.

REFERENCES

1. F. Auracher, H. Boroffa, and R. Th. Kersen, Technical Digest of the Integrated Optics Conference, January 12-14, 1976, Salt Lake City, Utah, Paper MD-1.

2. M.G.F. Wilson, C.W. Pitt, R. Manku, A.O. de Oliviera, and O. Parriaux, Electron. Lett. 12, 434 (1970).

3. G.L. Tangonan, L.E. Gorre, and D.L. Persechini, Optics. Comm. 27, 356 (1978).

4. G.L. Tangonan, O.G. Ramer, L.E. Gorre, H.R. Friedrich, C.K. Asawa, M.K. Barnoski, and D.L. Persechini, Topical Meeting on Optical Fiber Communications, March 6-8, 1979, Washington, D.C., Paper WG2.

5. G.L. Tangonan, O.G. Raner, H.R. Friedrich, C.K. Asawa, D.L. Persechini, and L.E. Gorre, Technical Digest of the Optical Communications Conference, Amsterdam, The Netherlands, September 17-19, 1979, Paper 21.5.

6. G.H. Chartier, P. Jassaud, A.D. de Oliviera, and O. Parriaux, Electron. Lett. 14, 763 (1979).

7. G.H. Chartier, P. Jassaud, A.D. de Oliviera, and O. Parriaux, Electron. Lett. 14, 132 (1978).

8. T. Izawa and H. NaKagome, Appl. Phys. Lett. 21, 584 (1972).

9. G.L. Tangonan and D.L. Persechini, to be published.

10. G. Chartier, P. Collin, A. Guez, P. Jaussand, and Y. Won, Appl. Opt. 19, 1092 (1980).

11. O.G. Ramer, Appl. Optics 19, 1294 (1980).